NAVAL POSTGRADUATE SCHOOL

MONTEREY, CALIFORNIA

THESIS

STRUCTURAL ANALYSIS AND OPTIMIZATION OF THE SUPPORT DEVICES USED FOR A PROXIMAL FRACTURE OF THE FEMUR

by

Richard A. Smith

December 2008

Thesis Advisor:	Young W. Kwon
Second Reader	Stephen C. Brawley

Approved for public release; distribution is unlimited

THIS PAGE INTENTIONALLY LEFT BLANK

REPORT DOCUMENTATION PAGE			*Form Approved OMB No. 0704-0188*
Public reporting burden for this collection of information is estimated to average 1 hour per response, including the time for reviewing instruction, searching existing data sources, gathering and maintaining the data needed, and completing and reviewing the collection of information. Send comments regarding this burden estimate or any other aspect of this collection of information, including suggestions for reducing this burden, to Washington headquarters Services, Directorate for Information Operations and Reports, 1215 Jefferson Davis Highway, Suite 1204, Arlington, VA 22202-4302, and to the Office of Management and Budget, Paperwork Reduction Project (0704-0188) Washington DC 20503.			
1. AGENCY USE ONLY ***(Leave blank)***	**2. REPORT DATE** December 2008	**3. REPORT TYPE AND DATES COVERED** Master's Thesis	
4. TITLE AND SUBTITLE: Structural Analysis and Optimization of the Support Device used for a Proximal Fracture of the Femur			**5. FUNDING NUMBERS**
6. AUTHOR(S) Richard A. Smith			
7. PERFORMING ORGANIZATION NAME(S) AND ADDRESS(ES) Naval Postgraduate School Monterey, CA 93943-5000			**8. PERFORMING ORGANIZATION REPORT NUMBER**
9. SPONSORING / MONITORING AGENCY NAME(S) AND ADDRESS(ES) N/A			**10. SPONSORING / MONITORING AGENCY REPORT NUMBER**
11. SUPPLEMENTARY NOTES The views expressed in this thesis are those of the author and do not reflect the official policy or position of the Department of Defense or the U.S. Government.			
12a. DISTRIBUTION / AVAILABILITY STATEMENT Approved for public release; distribution is unlimited			**12b. DISTRIBUTION CODE**

13. ABSTRACT (maximum 200 words)

The support system for a proximal fracture of the femur is studied by means of the finite element method. The support system of the Gamma III by Stryker is used for this study due to the versatility and simplicity of the system. The variance of each system was modeled to validate the results. Parametric studies between the models were conducted and design improvements were then tested against the existing parameters. Given the material properties for the Ti-6 AL-4V support system and bone, the models were considered under two different load conditions. From these results, a recommendation can be made to the manufacturing and medical community as to the effective use of the Gamma III nail implant system for a proximal fracture in the femur.

14. SUBJECT TERMS Finite Element Method, Femur, Proximal Fracture, Gamma Nail			**15. NUMBER OF PAGES** 103
			16. PRICE CODE
17. SECURITY CLASSIFICATION OF REPORT Unclassified	**18. SECURITY CLASSIFICATION OF THIS PAGE** Unclassified	**19. SECURITY CLASSIFICATION OF ABSTRACT** Unclassified	**20. LIMITATION OF ABSTRACT** UU

NSN 7540-01-280-5500 Standard Form 298 (Rev. 2-89)
Prescribed by ANSI Std. 239-18

THIS PAGE INTENTIONALLY LEFT BLANK

Approved for public release; distribution is unlimited

STRUCTURAL ANALYSIS AND OPTIMIZATION OF THE SUPPORT DEVICE USED FOR A PROXIMAL FRACTURE OF THE FEMUR

Richard A. Smith
Lieutenant, United States Navy
B.S., Campbell University, 1995

Submitted in partial fulfillment of the
requirements for the degree of

MASTERS OF SCIENCE IN MECHANICAL ENGINEERING

from the

NAVAL POSTGRADUATE SCHOOL
December 2008

Author: Richard A. Smith

Approved by: Young W. Kwon
Thesis advisor

Stephen C. Brawley
Second Reader

Approved by: Knox T. Millsaps
Chairman, Department of Mechanical and Astronautical Engineering

THIS PAGE INTENTIONALLY LEFT BLANK

ABSTRACT

The support system for a proximal fracture of the femur is studied by means of the finite element method. The support system of the Gamma III by Stryker is used for this study due to the versatility and simplicity of the system. The variance of each system was modeled to validate the results. Parametric studies between the models were conducted and design improvements were then tested against the existing parameters. Given the material properties for the Ti-6 AL-4V support system and bone, the models were considered under two different load conditions. From these results, a recommendation can be made to the manufacturing and medical community as to the effective use of the Gamma III nail implant system for a proximal fracture in the femur.

THIS PAGE INTENTIONALLY LEFT BLANK

TABLE OF CONTENTS

THIS PAGE INTENTIONALLY LEFT BLANK

LIST OF FIGURES

LIST OF TABLES

THIS PAGE INTENTIONALLY LEFT BLANK

ACKNOWLEDGMENTS

I would like to acknowledge all the people that were supportive during this process. First, I would like to thank my parents for believing in me and pushing me when I was younger. Second, I would like to thank Summer Lynch for all her patients and proof reading. In addition, I would like to give a vast amount of gratitude to Professor Kwon for his patients, mentorship and friendship. I would also, like to thank Dr. Brawley for the opportunity to work with him on this project.

THIS PAGE INTENTIONALLY LEFT BLANK

I. INTRODUCTION

In the United States, there are about 63 women per 100,000 and 34 per 100,000 intertrochanteric fractures among the elderly population. Some associated factors leading to a patient sustaining an intertrochanteric fracture are advancing age, increasing number of comorbidities, increased dependency in activities of daily living and a history of other oseoporosis related fractures [1]. Intertrochantric fractures in younger individuals are associated to high-energy injury. Some examples of high-energy injuries are motor vehicle accident and fall from a height. In elderly patients, 90 percent of intertrochanteric fractures occur from simple falls. An individual must land on or near the hip for the energy to be transmitted to the proximal femur. In elderly individuals are more likely for this type of fracture due to their deteriorating strength and reaction times being too slow [1].

The study of the background has shown many advances in the support system. Some seem to be an improvement; others seem to be a new method of accomplishing the same goal. While reviewing many of these support systems, it has been found that there have been a vast number of changes mad in the design without relevant support. For example, in Figure 1 and 2 the Russell-Taylor reconstruction nail is a dual nail system in the femoral head that acts as a support and transfer beam to the nail that is embedded in the femur. In Figure 3, 4 and 5, there are a number of apparent issues with the support system and the integrity that is maintained in the femur [2]. Other support systems are in favor of long femoral nails verse short and vice versa. In researching these design criteria, little supporting data exists as to why one system was chosen over another, for proximal femur fractures.

The addition of a radius of curvature is a notable evolution of the femoral support system. In the beginning of the design of these systems, a long cylindrical shaped nail was used as the main support of the bone during the healing process. As shown in Figure 6, an early design with this cylindrical nail, these designs bought about the discussion of the natural shape of the femur [5]. In reviewing the femur, it became apparent that the

center channel of the bone has a natural curve. Therefore, to implant a straight cylinder support system required the removal of bone to allow the nail to fit. This not only proved to be hazardous, especially in elderly patients, but it also proved to be inefficient. In later designs, by implementing a radius of curvature ranging from 2 degrees to 4 degrees as shown in Figure 6, obstetric supply companies and surgeons are able to improve the implanted support nail [2]. In positioning the nail in place there is less bone removed. This is important not only in the integrity of the bone, but is also protective against additional mechanical stresses and new fractures at the distal aspect of the nail.

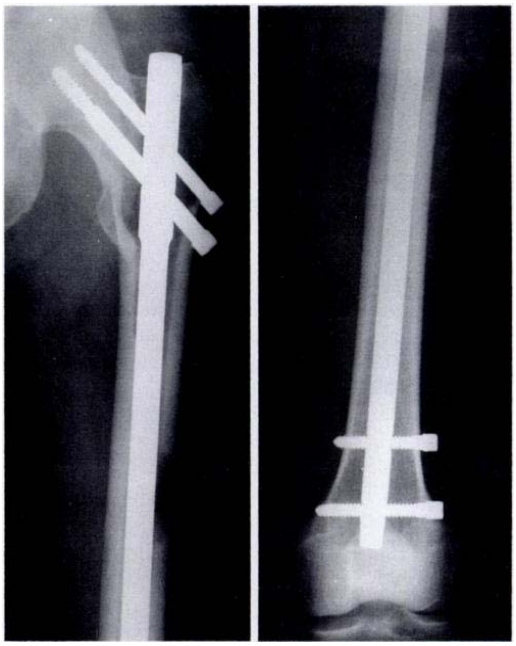

Figure 1. Russell-Taylor Reconstruction Nail [2]

Figure 2. Broken Implant [2]

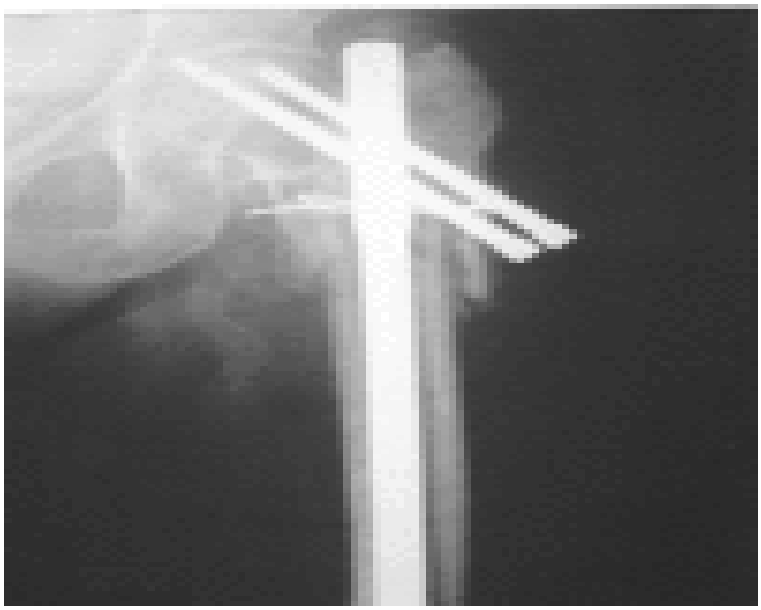

Figure 3. Z Phenomenon “Lag Screws backing out” [2]

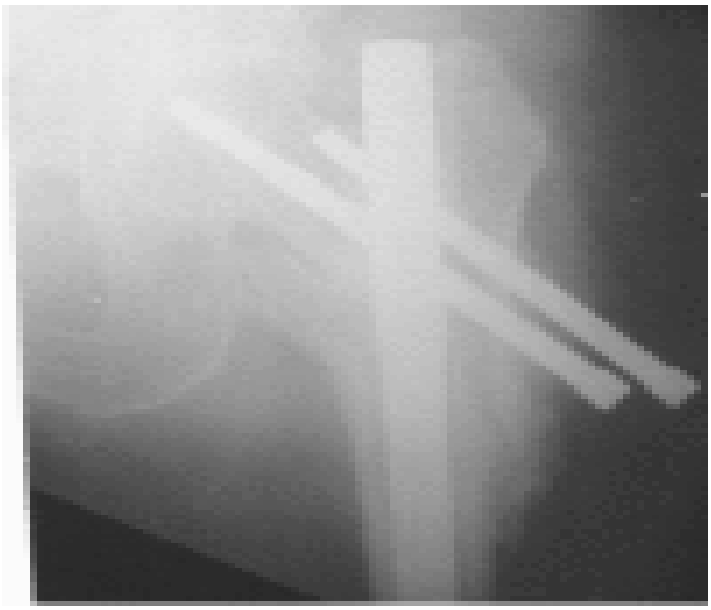

Figure 4. Reverse Z type phenomenon [2]

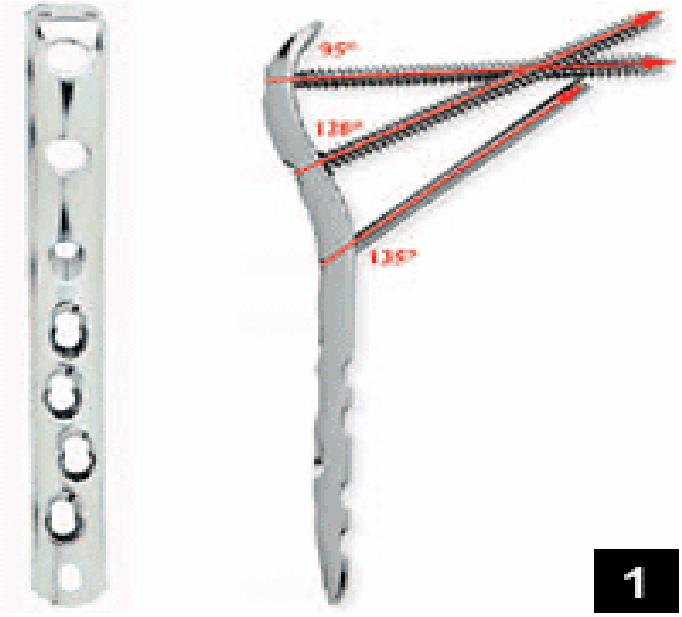

Figure 5. Another Type of Femur Support Nail [2]

The successes and failures of these support systems lead to improvements in existing design systems. The Gamma III Implant system™ is one of the least invasive support systems on the market. Along with the operative advantages, the Gamma III is a versatile system that can be configured to meet the specific needs of different patients.

The rational behind this study is to determine if the adjustability of the system is mechanically advantageous for surgical treatment of a proximal femur fracture. The primary concern of this study is to place each of the lag screw configurations under identical load, while adjusting the distal screw placements in accordance with given guidelines. This will determine if the improvement is advantageous in a fabricated gamma nail while giving the surgeon an ability to determine which distal screw configuration to utilize. The ultimate goal of the study is to illustrate how the von Mises stress and the shear stress are different for each lag screw configuration. However, these stresses can be minimized by choosing different distal pin configuration.

Figure 6. Gamma nail with curvature [3]

THIS PAGE INTENTIONALLY LEFT BLANK

II. BACKGROUND

A. FINITE ELEMENT ANALYSIS/ METHOD

1. Introduction to Finite Element Analysis/ Method

Finite Element Analysis (FEA) or Finite Element Method (FEM) is a relatively new method for solving complex engineering and mathematical problems. Since the 1940s, this method has evolved into the method of choice for computational analysis. In the early years, the finite element method was limited to the manpower available to solve large matrices. However, as technology has evolved FEM has evolved into a computational jug naught. This process is now only limited by the capabilities of the available hardware to solve matrices that can go out to machine epsilon. FEM is a part of many engineering applications such as structural mechanics, heat transfer, fluid flow, electromagnetic, blade design in orthopedic design for implants and prosthetics. It has become a key part of the design and refinement processes in engineering.

2. History of Finite Element Analysis/ Method

Courant is the mathematician credited for the formulation of the finite element method. In 1943, a paper was published in which Courant used piecewise polynomial interpolation by subdividing into triangular sections to solve a torsion problem [4]. It was not until the 1950s that significant steps were taken by Boeing to utilize the finite element method to model stress elements in commercial application, such as airplane wings. However, in 1956, Turner, Clough, Martin and Topp revealed that the original FEA method was established in 1930s by a structural engineer named Hrenikoff. Hrenikoff looked at two stress problems to determine the best way to solve them. First were the stress components in a loaded truss. Second were the stress components in a loaded flat plate. The loaded truss problem can be solved with simple statics procedures, which was limited to a finite number of interconnections. Hrenikoff looked at the problem of a loaded flat plate, which presents an infinite number of interconnections.

Therefore, Hrenikoff proposed to split the sections or elements with a finite number of nodes. This allowed for an object with infinite number of interconnections to be solved by conventional means. Turner, Clough, Martin and Topp further developed these ideals in their paper from 1956. However, in 1960, Clough first presented the term as "finite element method."

Advancements in the FEA/FEM field have only improved on the initial method founded in the 1930s. With advancements of the methods, there have also been advancements on the application of this process. FEA/FEM has evolved from a pure structural modeling and solving method to encompass other disciplines in the engineering and science fields. Examples of these are thermodynamics, biomechanics, fluid flow and many more. FEA /FEM are also benefactors of the advancement of technology. As computer processing advancements take place, it allows the FEA / FEM programs to compute more advance structures to greater accuracy. With the advancement of computer software such as computer-aided design (CAD) and computer-aided manufacturing (CAM), computational software producers have incorporated these graphic interfaces into their programs. Introducing these capabilities and advancements has increased the use of finite element modeling in many disciplines, thereby improving efficiency, reducing research time, and reducing the errors made in the design process.

3. Basic Steps in the Finite Element Method

The first step in utilizing the finite element method is to discretize a continuum problem in to a finite problem. This means to break down an infinite number of unknowns into a know number. Through this process a given area, a finite number of nodes and elements represents region or volume of an object. By placing these nodes and elements, an accurate representation of the area, region or volume is able to be studied. Then interpolations or approximation functions are used for the interpolation of the element. Most FEM solvers use polynomial interpolation limiting the polynomial is to the number of nodes in each element. These functions are known as shape functions. Figure 7 is an example of how a simple structure is discretized.

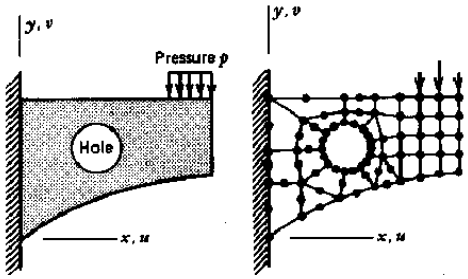

Figure 7. Dicretizing an object [5]

In using a FEA/ FEM solver, not only are the number of nodes and elements important in the accuracy of the results, but also the type of interpolation chosen. In many solvers, the type of element utilized determines the method used to solve the problem. Continuity of the mesh used to discretize the geometry is important criteria in receiving accurate results is finite element analysis.

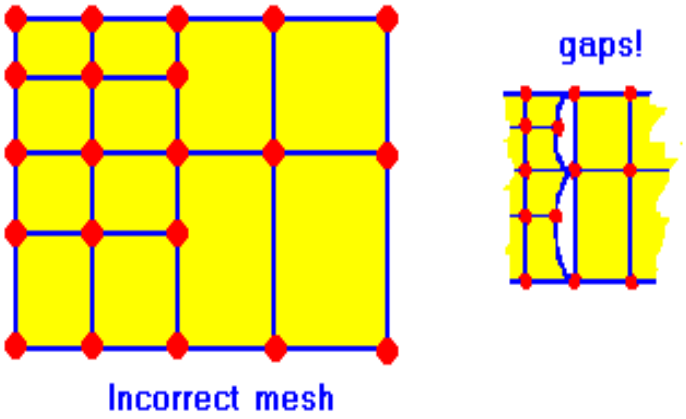

Figure 8. Incorrect Meshes [6]

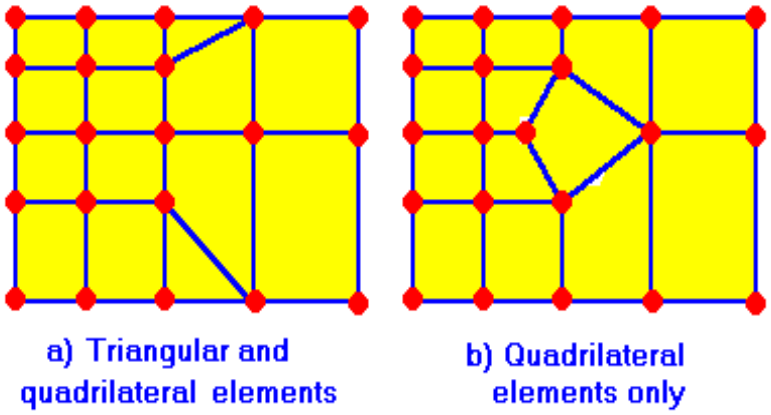

Figure 9. Correct Meshes [6]

Finite element analysis has several methods for solving given problems. These methods are weighted residual method, variation method, and direct approach. The direct approach is only able to solve elementary problems, which is based on the stiffness matrix for structural analysis. This method, even though effective for elementary problems, can be utilized to solve more complex one. This is accomplished by breaking down the complex geometry into elementary problems, with emphasis being placed on nodes that intersect. By utilizing this concept the designer/ engineer is able to determine a stiffness matrix for the give part of that structure. Then by combining the matrices of the parts, the stiffness of the entire structure can be determined. This method has become known as the direct stiffness method and was the first method utilized for solving finite analysis [7].

The variational approach is represented by calculus variations. The variational method utilizes both derivation and integral operators. By looking at equations one thru five, the finite element analysis can be related to natural boundary conditions known as the Neumann boundary, seen in equation two. This method is utilized with total potential energy functions. [7], [8]. Unlike the direct method, this method can be applied to complex shapes that are governed by the variational function [7], [8].

The most versatile and commonly used method for solving finite element analysis is the weighted residual method. In cases like heat transfer and fluid mechanics,

where functions cannot be defined the weight residual method can be used by the incorporation of a trail function. By utilizing this method, there are limitless applications because there is not set defining function like in the direct and variational methods [7], [8].

However, no matter which method is used, the basic steps for formulating the finite element analysis are the same. The first step is to develop a model of the problem to solve. In conducting this step all parameters must be defined; boundary conditions, initial conditions, geometric image, material properties, the domain and the loads placed on the object. Users must minimize the analysis as much as possible. The main driving factor for these simplifications is the computational power at the user's disposal. If the computational power is unlimited, the model should be maximized. However, in a research situation where computation power is limited, the model should be minimized as much as possible.

Once these initial parameters are defined, the model needs to be discretized or meshed. While meshing the model, the factors to take into account are the size of the mesh, shape, number of nodes and the number of elements in the model. While meshing, great care should be taken to ensure uniformity. The following Figure 9, show examples of elements that should and should not be used when meshing a geometry [6].

The final stages of conducting a finite element analysis consist of choosing an analysis type and verifying the results for accuracy. By choosing the type of analysis to be accomplished, it dictates the method to be used to achieve the results; i.e. direct, variational or weighted residual method; of the finite element model. Once this process is successfully completed, results must be checked for accuracy. The ways to conduct such checks are to refine the elements and/or to conduct a parametric comparison [6], [7], [8]. In addition, conduct a parametric comparison by utilizing graphical representation. After the refinement process, graph the results and check for convergence to verify accuracy.

B. FEMUR

"The femur is the longest and strongest bone in the human body."[9] Being the longest and the strongest bone in the human body, it transfers the weight of the upper torso to the lower extremities. The femur is angled downward and medialward to allow for the weight transfer of the upper torso to the lower extremities putting them into the line of gravity of the body [9]. The proximal femur contains the head (caput femoris), the neck (collum femoris) and the greater and lesser trochanter, see Figure 10 [9].

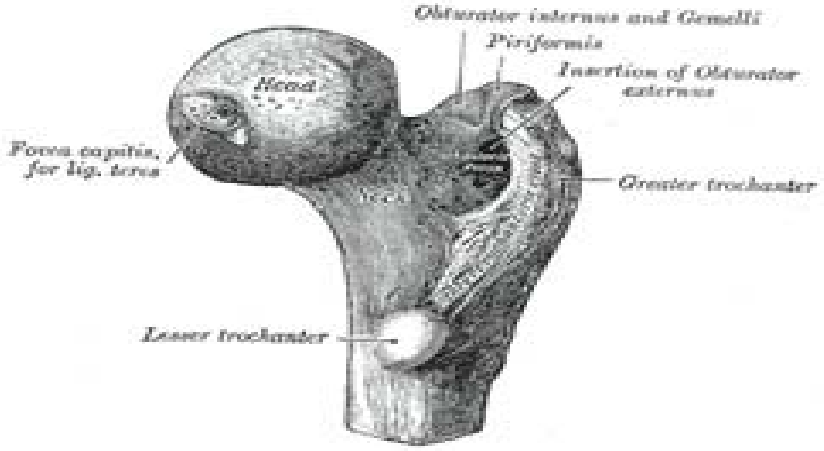

Figure 10. Proximal Femur [9]

The Head of the femur is smooth at approximately three-fourths of a sphere or the ball on the proximal extremity and is covered with cartilage. The head sets slightly upward, forward and medialward, "the greater part of the convexity being above and in front [9]." The only exception to the smooth nature of the head is the fovea capitis femora, which is where the ligamentum teres attaches. The fovea capitis femora is shown in Figure 10 [9].

The neck or collum femoris is the angled portion that connects the body and the head. This bone is a flattened pyramidal bone that forms a lateral angle from the medialward. The angle of the neck is greatest as an infant and decreases to an approximate angle of 127 degrees as an adult [10]. This angle varies between every individual and varies with relation to stature. The neck also projects the head forward and medialward at angle of 12 to 14 degrees. The angle is dependent of sex, stature and

development of the individual. The neck is not uniformed in shape as it connects the head to the lesser trochanter. As seen in Figure 7, the neck is flatter on the lower proximity to the lesser trochanter, which gives a one-third increase in diameter than the anterior-posterior edges. The anterior surface is perforated by vascular foramina and is marked by shallow grooves. These shallow grooves are best seen in the elderly and "lodges the orbicular fibers of the capsule of the hip-joint [9], [10]." The posterior surface is smooth and is broader and more concave than the anterior surface. The hip joint is attached about one cm above the intertrochanteric crest. Finally, the neck is made of two borders: the superior and inferior borders. The superior border is thick, short and ends laterally at the greater trochanter. The trochanters are the attachment points of muscles, which allow for the movement of the hip. The inferior border is long, narrow, curves backwards and ends at the lesser trochanter.

The greater trochanter or trochanter major is located at the upper portion of the neck and the body as seen in Figure 10 [9], [10]. It is located lateralward and backwards, it is about 1 cm lower than the head. The greater trochanter is broken down into two surfaces and four borders. "The lateral surface is broad, rough, convex and marked by a diagonal impression, which extends from the postero-superior to the antero-inferior angle, and serves for the insertion of the tendon of the Gluteus medius [9], [10]." The medial surface has a deep depression called the trochantric fossa (digital fossa) that allows for the insertion of the Obturator internus and Gemelli. The superior border is thick, irregular and marks the insertion for the Piriformis. The inferior border is on the base line of the trochanter lateral with the body, "it is marked by a rough, prominent, slightly curved ridge, which gives origin to the upper part of the Vastus lateralis [9]." The Gluteus minimus is attached to the lateral portion of the anterior border. The posterior border is the last border of the greater trochanter; it is a free, rounded edge. The lesser trochanter (trochanter minor) is a conical eminace on the inferior and posterior aspect of the proximal femur [9], [10].

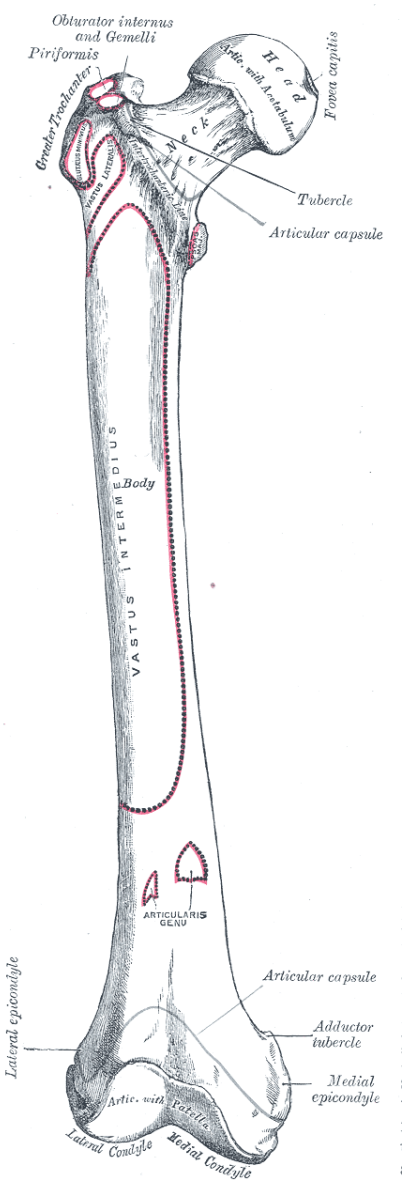

Figure 11. Full Femur [9]

C. TI-6AL-4V TYPE II ANODIZED

The medical industry has switched from using stainless steel to some form of titanium for implant procedures in the last 20 years for many orthopaedic procedures. The titanium alloy that is of main interest is Ti-6 Al-4 V Type II Anodized. The name indicates that the main material in the alloy is titanium by approximately 85 percent with 6 percent aluminum, 4 percent validum as the main elements and the remainder with

other various elements. Titanium alloys are metals that are very expensive to produce but very strong compared to other metals. Another reason for using titanium alloys over titanium element is the ability to enhance the material's properties. Engineers try to utilize materials that are able to resist traits that the material will be subjected to in the invention. Therefore, the use of titanium alloys in the medical industry is to resist the environment of the human body.

The medical industry uses Titanium alloys in the human body for many reasons. One of the main reasons for utilizing titanium alloys is their resistance to pitting, general and crevice corrosion. Another reason for the use of titanium and its alloys is its ability to generate a protective coating, Titanium Oxide. This coating allows the metal to resistant to the fore mentioned corrosions. In addition, titanium is resistant to the chemicals that are produced in the body; such as ammoniam, sulfides, nitrites, ferrous compounds, organo-sulfur and acidic compounds produced by aerobic microorganisms in the body [11], [12]. Titanium and its alloys are less likely to be rejected by the body given that they are not biotoxic and biological growth occurs on and into the metal.

One of the most important properties for using Ti-6Al-4V Type II anodized alloy in an implant structure is its high strength and relatively low density. The alloy that is used has tensile yield strength of 828 MPa, compressive yield strength of 828 MPa and a tensile ultimate strength of 895 MPa. The density of this material is 4420 kg/m^3 [16]. The process in which the metal is made also improves the fatigue strength of the metal. Type "II" anodizing is an electrolytic process that causes a film to build up on the surface of the metal. This process does not add layers to the surface of the metal but penetrates the metal. This process is very difficult to uncover due to the proprietary nature of the chemicals involved. This process gives the manufacturers the ability to control the procedure used to make the titanium alloys, therefore giving a higher yield. Through this process, the titanium alloy is able to be enhanced. The fatigue stress can be increased by 15 to 20 percent enhancing the metal's ability to be welded. The surface of the material is improved by about 50 percent, reducing imperfections. Finally the anti-galling and wear characteristics are improved.

Titanium and its alloys are unique in that they are resistant to ductile deformation. This characteristic is related to the process in which the titanium under goes its phase transformation in the production process. Titanium utilized goes through an alpha-beta phase transformation that improves the strength and ability to resist ductile deformation. In looking at the stress-strain curve of this alloy, the ductile region is almost plateau in nature. This depicts the ability to resist ductile deformation at a high stress and high strain condition, but fails under ductility when the limits are exceeded. By studying the same graph, the brittleness of the material can be determined. The alloy in question is shown in the following stress-strain curve, thus showing the brittleness and ductility of the material.

Another process for the improved strength of this material is the phase transformation that the material undergoes during production. An alpha-beta phase transformation is a two-phase transformation that increases the strength and ductility of the alloy. During the process, beta stabilizers are added to titanium in order to allow for the addition of other elements during the beta phase. By adding the beta stabilizers, the metal is allowed to persist to below the transus temperature down to room temperature. By conducting heat treatments at temperatures in the alpha-beta phase region and a quenching process improves the materials strength. This process is followed by an aging cycles that occurs at lower temperatures. The aging cycling causes fine alpha particulates to form from the metastable beta. This strengthens the material more than an annealing process. While this strengthens the material, the ductility of the material is slightly decreased [13].

D. LITERATURE REVIEW

Publications addressing a fracture in the femur are easily accessible. However, few publications discuss the limitations of component failure, modeling and loading of a femur. The articles reviewed, “Effect of force direction on femoral fracture load for two types of load conditions,” “Finite element study trochantric gamma nail for a trochantric fracture,” “Finite element analysis of a Gamma nail within a fractured femur,” and “Prevention of fracture at the distal locking site of the Gamma nail” address such areas.

In the article entitled “Effect of force direction on femoral fracture load for two types of load conditions” by Keyak, Skinner and Flemming published in the Journal of Orthopaedic Research, finite element analysis of four femur specimens are discussed. The specimens were placed under two different loads: one simulating a fall and the other mimicking normal activities. The loads were applied to each femur sample and then computed the greatest applied loads and lowest fracture loads. The simulations of these loads were applied to various parts of the femoral head. The portions that the loads are applied are representative of various degrees off the center of the given direction, anterior and posterior direction with the alpha load applied 15 degrees off the median line and beta twenty-five degrees off the median line. This article is able to correlate the same load tendencies over a diverse sample group. Reviewing this article confirmed that fractures could be predicted but not all load conditions can be simulated. Thereby, making it impossible to predict which loads will cause a failure [14].

In the “Finite element study of trochanteric gamma nail for trochanteric fracture,” finite element studies are discussed as the parts in the trochanteric gamma nail. This study utilized the data taken from the analysis conducted under various loads to produce stresses and displacements. This article, one of the few, reviews the entire implant system and studies it on an individual level. A number of the findings in this article appear to be the basis for various design decisions within Stryker’s Gamma implant system. The article findings state that the titanium model reduces stress concentrations by 30 percent of the stainless steel models. Within this journal article the authors determine that the lag screw and distal screws are the critical elements of the implant system. The von Mises stress is the main driving factor for determining if the gamma nail is optimized. The authors also felt that the displacement is very important in determining the optimization. The displacement can be correlated to the thickness of the gamma nail. As the gamma nail’s diameter is reduced its stiffness is also reduced, thus making the gamma nail more susceptible to failure [15].

In subtrochantric fractures there are numerous failures, even though the implant system is being used. “Finite element analysis of a Gamma nail within a fractured femur” discusses this failure and what can be done to minimize it. In conducting this

analysis, it is imperative to determine the stress critical components of the implant system. Wang, Yettram, Yao and Procter determine which component is critical and discuss a configuration to minimize it [16]. The loadings used in this paper illustrated diversity not available within other reviewed articles. The major areas of concern discussed in this article are the insertion holes for the lag screw and the distal screws. These areas are the most vulnerable to fractures in the Gamma nail. The authors addressed the loading of the Gamma nail from a practical yet diverse manner, thereby drawing from the loading condition used by Wang, Yettram, Yao and Procter [16].

The "PREVENTION OF FRACTURE AT THE DISTAL LOCKING SITE OF THE GAMMA NAIL" discusses the importance of centre drilling the distal locking screws to the correct size in order to minimize stress fractures caused in the bone. The awl process decreased the required torsion known to cause a failure. Centre drilling did not reduce the torsion required for failure as much as using an awl process. The bottom line is drilling holes are stress riser and decreases the mean failure load. This research shows the importance of studying the results of placing torsional loads on the femoral head to determine the effect of the long gamma nail [17].

III. INTRODUCTION TO THE GAMMA III NAIL

The Gamma III Locking Nail is a third generation support system for a proximal fracture of a femur. This support series has been in existence for over fifteen years. Many of the improvements for this system are based on clinical research and feedback from the medical field. One of the key factors for the use and promotion of this system is the versatility of the system required by the medical professionals. Another advantage is the reduced invasiveness of the procedure on the patients, thereby reducing the recovery time and likelihood of infection. The Gamma III system is a complete system for the medical professional and patient. The Gamma III nail provides the necessary structural integrity to allow for proper healing of a proximal femur fracture and early abulatin by the patient.

A. PROPERTIES OF THE GAMMA III NAIL

The Gamma III Nail consists of two types of gamma nails: the short and the long nail. Both nails have the capability to adjust the lag screw to three angles: 120, 125 and 130 degrees, as seen in Figures 12 and 13. Both the short and long Gamma Nail has a proximal diameter of 15.5 mm and a distal diameter of 11 mm. In addition, both nails are constructed with a Type II anodized Titanium alloy (Ti-6Al-4V) and have a 4 degree M-L bend for valgus curvature. The end caps on both the short and long nail are offered in three sizes: standard, +5mm and +10mm. Both nails are compatible in that they both utilize the following parameters: lag screw diameter of 10.5 mm, lag screw lengths of 75-120 mm, distal locking screws diameter of 5mm and lengths of 25 to 120 mm able to be altered in increments of 2.5mm or 5mm. There are few differences between the two nails. The first and most obvious is the lengths: the short nail 180mm and the long nail ranges from 280 to 480 mm in increments of 20 mm. The short nail consists of on distal locking screw while the long nail can have up to two distal locking screws.

The distal locking system is one of the unique features that set the Gamma III system apart from the rest of the implant systems on the market. The short nail consists of one distal screw that can be put into the distal or static locking configuration. The

locking hole in the gamma nail is placed into a oblong hole of approximately 10mm in length. This creates a dynamic locking mechanism, which allows vertical movement of the gamma nail, thereby decreasing stresses observed in Quasi-static loads. The long nail's dynamic locking configuration is slightly different as shown in Figure 14. The dynamic locking system requires one distal screw in the lower portion of the oblong hole as shown in Figure 14. The secondary dynamization is set up in the following pattern shown in Figure 14. This is initially for slight movement in the gamma nail but if the nail is required to have dynamization then the upper distal screw needs to be removed. This configuration is utilized for allowing dynamization at some point after the initial healing process. The final configuration in the long nail is static locking shown in Figure 14. This is designed for no movement of the gamma nail.

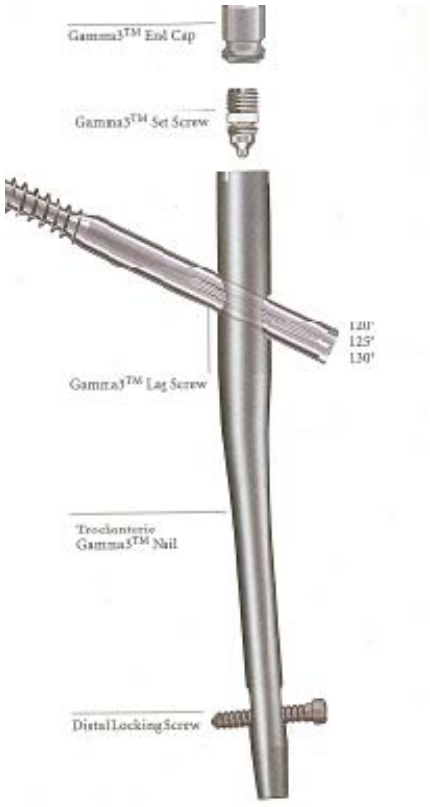

Figure 12. Short Nail Assembly [3]

Figure 13. Long Nail Assembly [3]

Figure 14. Distal Screw Configurations [3]

B. SURGICAL PROCEDURE:

The main purposes for using the Gamma III™ implant system are to stabilize a proximal femur fracture for healing and to minimize the invasiveness of the implant procedure. Using that knowledge, the first item that the surgeon must determine is which nail to implant. In Figure 12, the short Gamma nail is used for peritrochanter. Conversely, as shown in Figure 14, a long Gamma nail is used for subtrochantric fractures and pertrochanteric fractures [3]. The length of the long Gamma nail is chosen by either "preplanning using an x-ray of the femur as a template or by intra-operatively measurements, the usual method for determining the length during intramedullary nailing [3]."

In installing the Gamma III Implant system™, it is important that the patient is in an optimum position for the procedure. The patient is placed in a supine position on the fracture table. In this position, the fracture should be closed as anatomically as possible. If this is not achievable then the fracture must be reduced by an open reduction. If the fracture can be closed by the closed reduction, traction is applied to keep the leg straight, as in Figure 15. While traction is applied, the leg is rotated 10-15 degrees to complete the fracture reduction; an indication of this is that the patella is positioned horizontally or slightly inward. In this position, the intensifier can be positioned to maintain an A/P and M/L, as in Figure 16. The intensifier is positioned for the A/P and M/L views, maintaining proximal and distal views of the femur giving the surgeon the most feedback during the Gamma nail insertion.

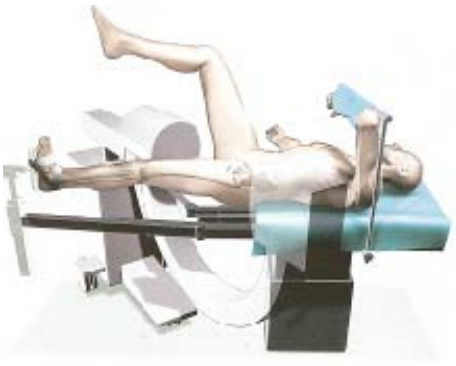

Figure 15. Positioning of the Patient [3]

Figure 16. Use of Intensifier for alignment [3]

The entry point is at the junction of the anterior third and posterior two-thirds of the greater trochanter, Figure 17. The first incision is made of the appropriate length from the greater trochanter in the direction of the iliac crest [3]. Once the incision is made, a cannulated curved awl is used to open the medullary canal. When reaming the medullary canal, the proximal end must be reamed to at least 15.5 mm to accommodate the proximal end of the gamma nail. After about 90mm, the remainder of the medullary canal should be reamed to about 13.5 mm to accommodate the distal end of the gamma nail. During this process, the initial reaming is at 9 mm and increased incrementally by .5 mm until the desired diameter is obtained.

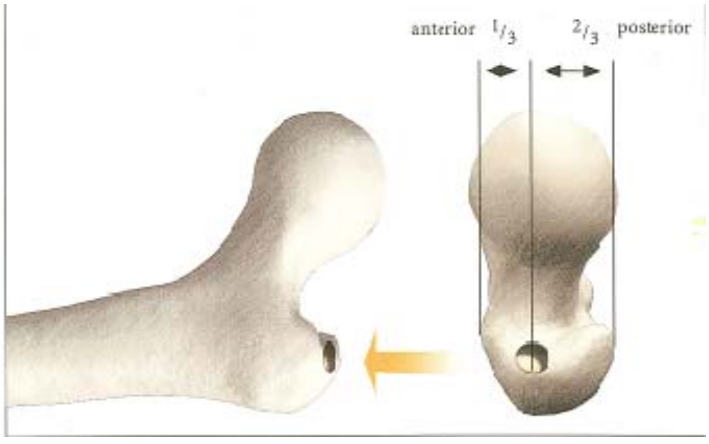

Figure 17. Position of Gamma Nail in Greater Trochantric[3]

Now that the medullary canal is ready for the implant of the gamma nail, the targeting tool must be assembled. This tool is one of many advantages of using the Gamma III Implant system^{TM}. The assembly of the targeting device is relatively simple. First, the targeting sleeve and knob are assembled by aligning the arrow on the targeting sleeve with the spot on the knob as in Figure 18. Then rotate clockwise one-third of a turn as shown in Figure 18. Finally, the targeting sleeve and knob assembly is joined with the targeting arm. The long arrow on the targeting sleeve assembly and the targeting arm are aligned and joined, Figure 18. Once this is achieved, rotate the targeting sleeve assembly to align the appropriate holes, i.e. the lag screw angle or the appropriate distal screw combinations. Push the targeting sleeve assembly to the proximal end of the targeting arm to lock in place [3].

Figure 18. Targeting Tool [3]

Insertion of the Gamma III nail is done by hand to ensure that the gamma nail is not forced into place. First, the proper depth is checked using the image intensifier. Then the lag screw's position is checked with the ruler on the C-arm monitor. The lag screw should be placed centrally or slightly inferior in the femoral head and frontal plant as in Figure 19. The lag screw should also be centrally positioned in the femoral head as shown in Figure 21. Another tool that Stryker provides for the lag screw alignment is the "One Shot Device ™" [3]. This give the surgeon a view of the lag screw as it will sit in the femoral head, Figure 19. The tool makes it easy for the surgeon to determine the correct position of the lag screw in both the A/P and lateral views, along with the image intensifier, as shown in Figure 20 and 21 [3].

Figure 19. One Shot Device[3]

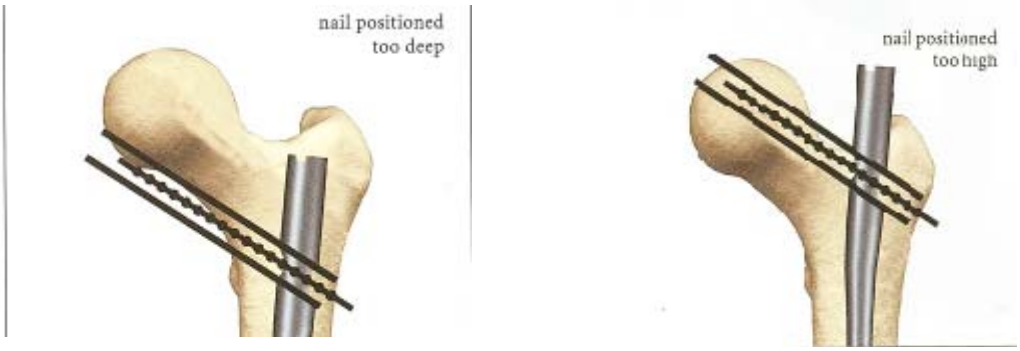

Figure 20. Incorrect Alignment of Gamma nail[3]

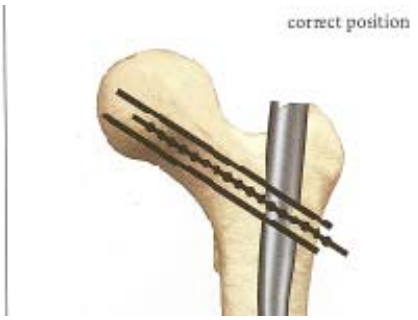

Figure 21. Correct Alignment of Gamma nail [3]

Insertion of the support nails is the final stage of this procedure. Since all of the alignment checks have been accomplished for the lag screw, the guide sleeve is inserted into the targeting arm and an incision is made at the contact point of the guide sleeve and the epidermis. The guide sleeve is pushed toward the bone until contact is made, at which point the guide sleeve is locked into place by turning the targeting knob clockwise. A measuring hole is drilled with the K-wire sleeve to determine the length of the lag screw, as shown in Figure 22. The hole for the lag screw is drilled to the determined length, which requires a 10mm space of cortical bone from the tip of the screw to the tip of the femoral head, as seen in Figure 23. The lag screw is then held rotationally in place by a locking tab. This tab allows the lag screw to slide but not rotate. The targeting arm, however, is no use in aligning the distal screws. These screws must be implanted without any aid other than visual aid provided by X-ray. The gamma nail's alignment is checked by x-ray prior to any incisions are made. Once the alignment is verified, an incision is made in the appropriate location. The drill is then place perpendicular to the femur. X-rays are again taken to ensure that the A/P and M/L alignment is correct to the hole that is being drilled. The configurations for the distal locking holes are shown in Figure 14**.** There are three distal screw configurations in the Gamma III nail; single screw dynamic locking, two screw dynamic locking and the static locking. The distal screws are inserted until contact and resistance is felt. The final step is to install the end cap once the distal screws are in place. Final assembly is shown in Figure 24 [3].

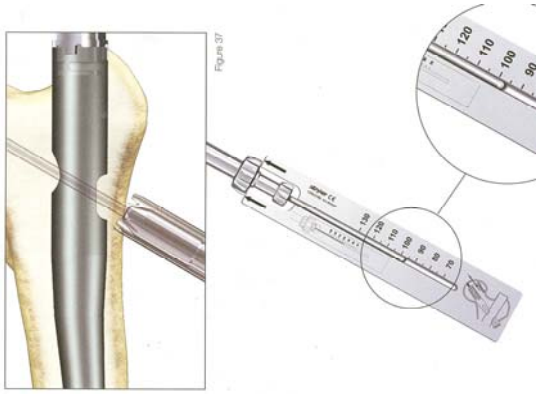

Figure 22. K-wire to measure the length of Gamma nail required[3]

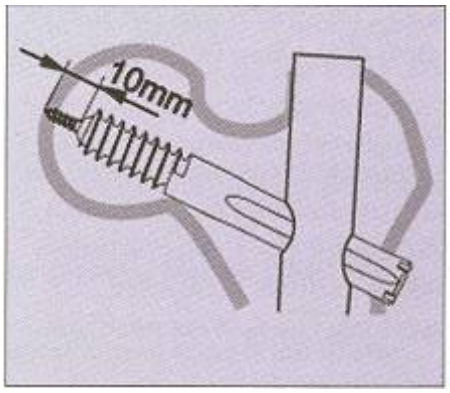

Figure 23. Desire depth in the Femoral Head [3]

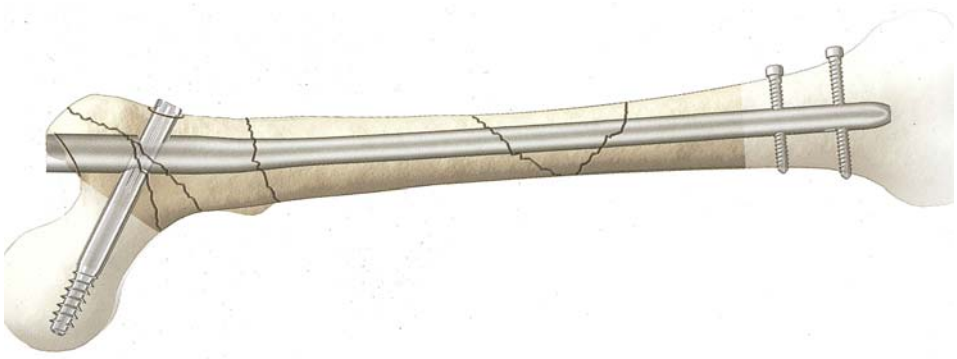

Figure 24. Complete Femur and Gamma III Implant system^{TM}[3]

THIS PAGE INTENTIONALLY LEFT BLANK

IV. MODELING

During this research, the ability to obtain a 3-D model of a femur that was generated in IGES format was not obtained. Therefore, the models were generated from scratch in Ansys, Workbench version 11.0. This model is a rudimentary copy of the model used by Wang, Yettram, Yao and Procter in their "Finite element analysis of a Gamma nail within a fractured femur" (Figure 25). The modeling process occurred in four distinct phases: geometric design, meshing, solving/simulation and generation. The software enabled a smooth transition between each phase.

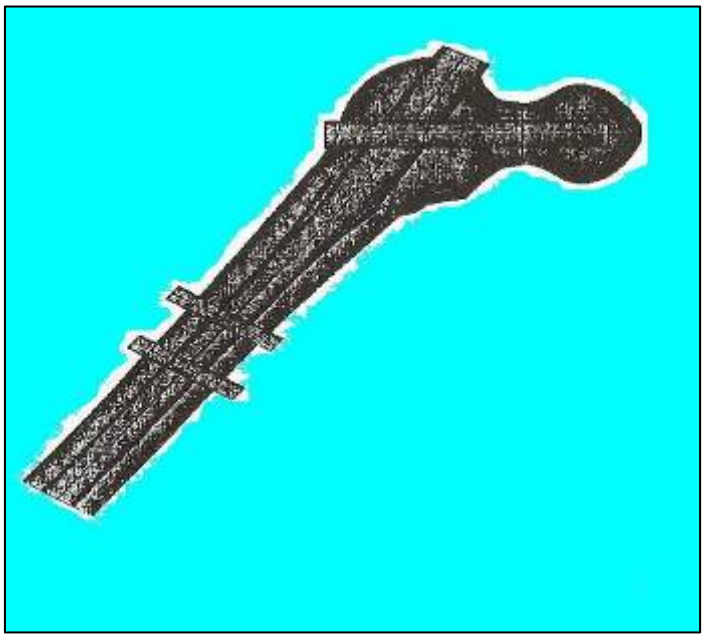

Figure 25. Reference Model [16]

A. MODEL DEVELOPMENT

The first phase of the Modeling is the geometric design. During this phase of the modeling many factors were taken into account. The first of these were deciding which way to set up the axis of design and loading. The relative axis of use in all of the models, as seen in Figure 26, sets the axis use in every model. In this axis format, the x-axis is equivalent to the M/L direction, the y-axis is the A/P direction and the z-axis is the S/I

direction. From this point, the geometric designs can be generated uniformly. The Gamma nail with a 4-degree curve M/L direction was the first model generated. This generation was conducted to model the nail in Figure 26. With the generation of Figure 26 and Figure 27, little to no discrepancies exists. Next, was the modeling of the lag screw and all three angles; 120, 125, and 130. As the lag screw's angle increased some adjustment was need to place the screw in the centerline of the neck and femoral head. .

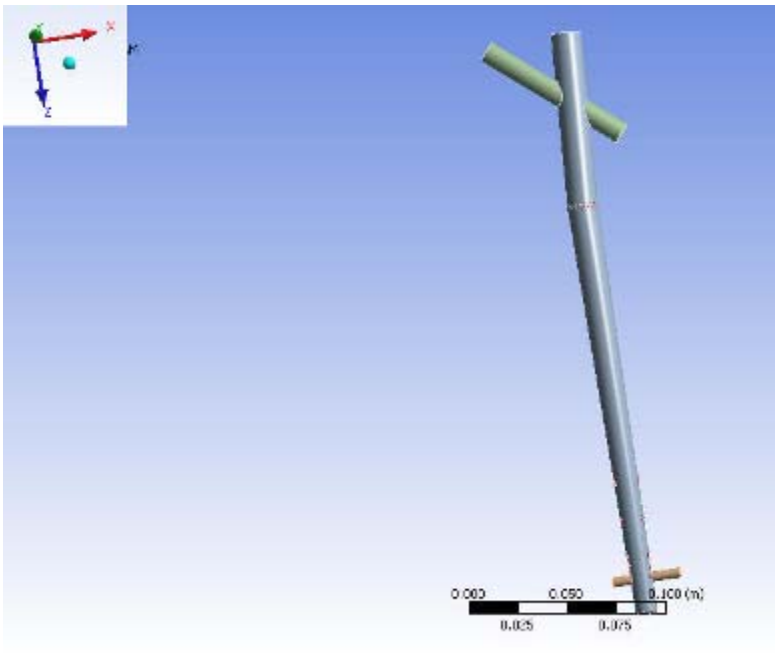

Figure 26. Gamma nail with coordinate reference

Once the gamma nail is generated, another file is used to generate the generic femur. The first portion generated is the diaphysis of the femur, which is approximately 330mm long. Then the proximal end of the femur is generated as a sphere, starting with the greater trochanter. The proximal femur can be easily generated and volume added to the femur diaphysis at a radius of 25mm. A sphere allows for ease of meshing this shape and transitioning to the diaphysis of the femur. The next section of the femur to be produced is the neck. The neck is generated to be 40 mm long and have an outer radius of 20 mm and an inner radius of 12mm. The neck is set at an angle of 120 to 130 degrees from the body, to account for anatomic variations. At the end of the neck is the femoral

head, the main load-bearing portion of the femur. The radius of the sphere utilized is 25mm. By setting this geometry, the simulation of the femur is to have the femoral head about 1-5 mm above that of the greater trochanter portion, see Figure 27. The distal end of the femur is simulated as a flat plate that is constrained to zero movement.

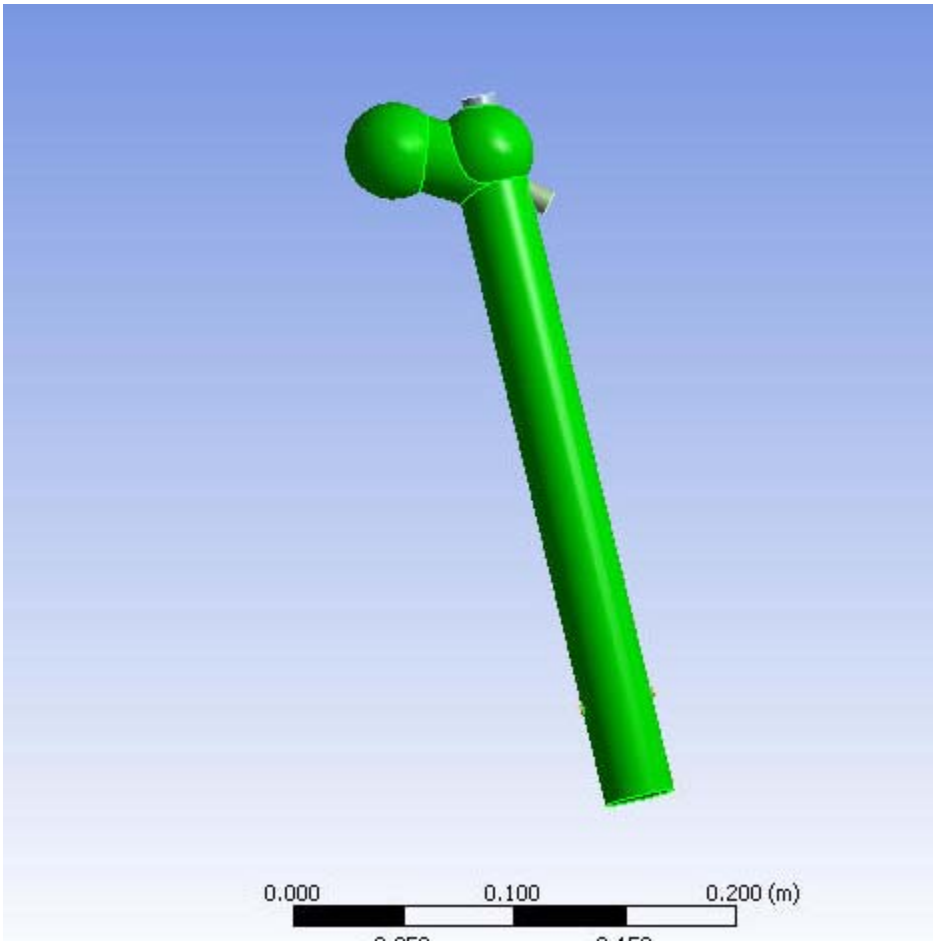

Figure 27. Model with bone and Nail

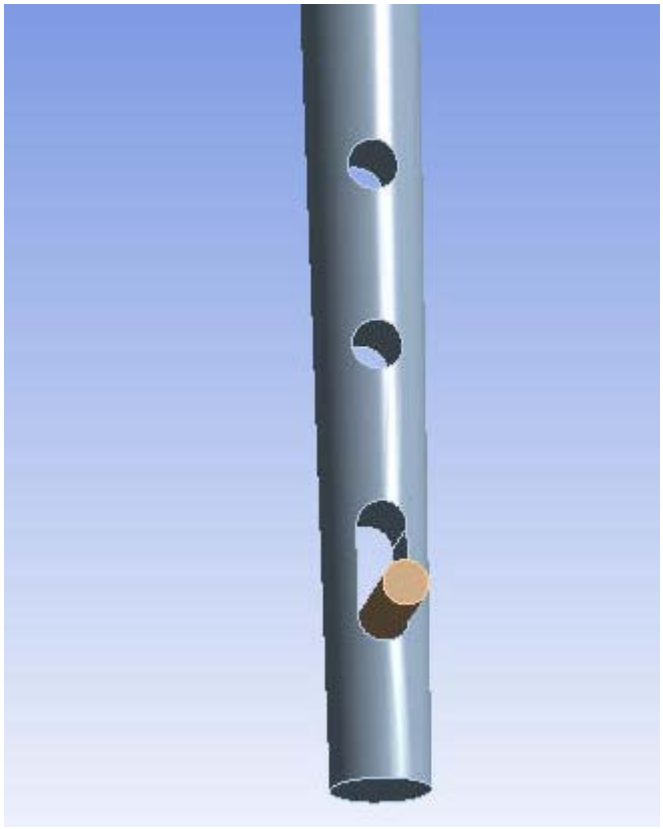

Figure 28. Distal holes modeled

An advantage of the software's ability is to work on generated planes and manipulate sketches on those plans. This was an important tool when lining the Gamma nail in the proper location of the greater trochanter. Once the gamma nail is set in the proper location, the nail needs to be rotated in the proper direction to line up with the medullary canal. The extrude function is utilized to remove the proper amount of the medullary canal to allow for the proper fit of the gamma nail. In this model, a uniformed canal was augured out of the medullary canal to allow for a uniform fit in all models and to allow for a uniform analysis of the models. In conducting this portion of the modeling, the gamma nail is placed in the proper direction to ensure that the curvature of the nail is in the M/L direction. At this point, the proper distal screw configuration can be generated, in accordance with Figure 12. In addition to the prescribed distal screw location for the Gamma III Implant system™, the experimental configuration is shown in Figure 28.

In placing the nail generations and manipulation into their proper location, it is imperative that each body-part is separated from those of other properties. The separate parts can be glued by Boolean operations after they are defined. To simulate the auguring and nail space relation ship, a hole that is 10 percent larger than the prescribed nail is extruded out and then the screw generated. This ensures that each of the screws are defined as independent bodies and produce a contact point with all the appropriate areas. The overall screw and screw/bone model is seen in Figures 26 and 27.

B. MESHING

The meshing section of the program is where the individual bodies are defined. These bodies are defined as either titanium alloy or bone. Titanium alloy is defined with the following parameters: 114 GPa Young's modulus, 828 MPa tensile strength, 895 MPa ultimate tensile strength, density of 4420 kg/m^3 and a Poisson's ratio of .3 [16]. The bone is defined by the following characteristics: 17 GPA Young's modulus for cortical bone, .3 Poisson's ratio and a density of 1900 KG/m^3 [16]. By selecting all of the areas of the geometry, the meshing function can be applied. Looking at the following Figure 29, one can see that the mesh of this geometry is very course. Conducting the same procedure, selecting all the bodies and adding a refinement function, the mesh is refined in all the bodies of the model, as seen in Figure 29. This meshing is uniform and aligns in transition points of bodies that are glued or merged together. Some of the areas that are meshed seem to be more concentrated with elements than others, this occurs primarily due to a transition from on geometric shape to another.

The femur utilizes the 10-node quadratic tetrahedron type mesh which contains to nodes per tetrahedron. This mesh is used given its ability to conform to the geometry being meshed and it gives the most nodal points per area for this geometry. While the Gamma III implant system^{TM} utilizes two types of meshing shapes, the 10 node quadratic tetrahedron is the element shape found in all of the geometric shapes of the model. It allows each element to contain 10 nodes. The overall geometry contains a multitude of nodes and elements that are shown in the Appendix for the complete number of nodes and elements for each type of model. To ensure its integrity, the mesh should be as fine as possible therefore depicting a realistic mathematical representation of the actual femur

and Gamma III implant system^{TM}. However, a compromise must be made between computational performance and realism of the model. The mesh generated in the models used for the parameterization of the Gamma III distal screws are representative to an actual model and not jeopardizing computational performance.

Figure 29. Examples of Meshing Coarse and Fine

C. CONTACTS

An important factor in modeling the femur with the Gamma III implant system^{TM} is to maintain a realistic model with the operative procedure. The conditions in which this operation takes place are not optimum enough to ensure direct contact in the screws. While the lag and distal screws are screwed into place, there are still areas in which the nail/screw and bone will move and come into contact. Therefore, this modeling is representative of a more conservative case looking at the contact between the gamma

nail, distal screw and bone. Both the lag and distal screws are generated with an initial gap of approximately .1 mm. In the contact model, the contact is modeled as a bonded contact. Bonded contact is defined as a "contact region that is bonded, then no sliding or separation between faces or edges is allowed" [8]. At this point, the regions act as one region known as "glued". This type of contact was chosen because the length of the model will remain the same, gaps in the contact region will be closed and initial penetrations will be ignored. This is ideal for linear solutions. The contact regions, for the most complex model, can be seen in the following Figures 30, 31, 32 and 33. The contact regions interact by quadratic triangular contacts and targets. These contact shapes allow for the transfer of forces between volumes. The standard contact displacement is 4×10^{-4} mm of movement between the two objects; contact surface and target surface. The defined contact surfaces in the model are located between the bone and the gamma nail, bone and lag screw, bone and distal screws, gamma nail and the lag and distal screws. In the complex fracture model, contact surface is also between the bone and bone at the lesser trochanter, as seen in Figure 30.

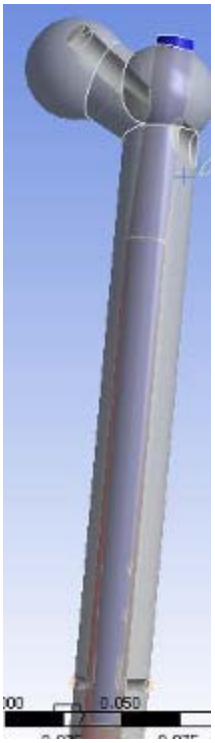

Figure 30. Contact Region 1 between Gamma Nail and Bone

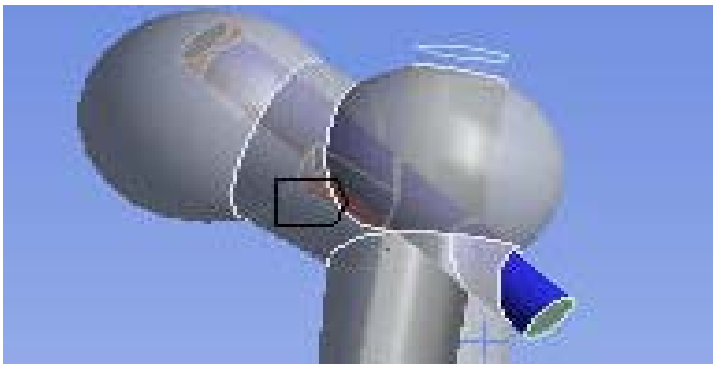

Figure 31. Contact Point 2

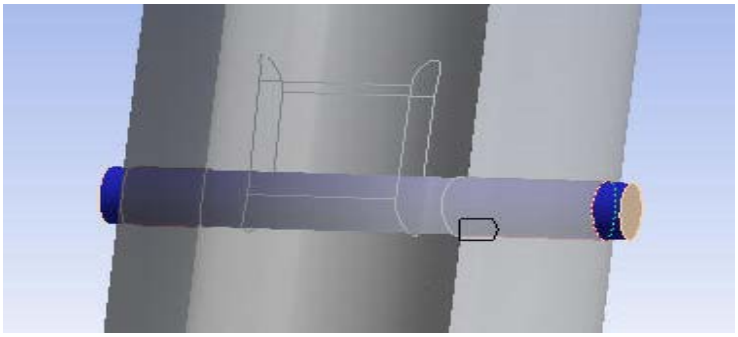

Figure 32. Contact Point 3

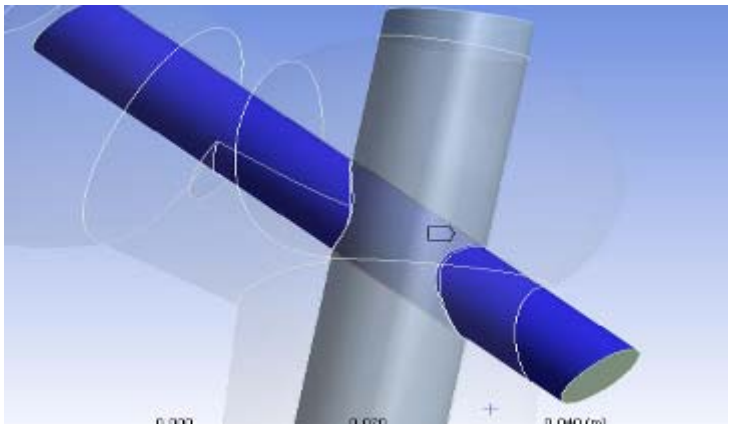

Figure 33. Contact Point 4

D. SIMULATION

The next phase is of the process determines the stresses and deformation. The type of loads and constraints applied defines the model. Three basic loads define the model. These loads represent forces from muscle, tendons and gravity during physiologic activities. The first load is three loads applied in the M/L direction and the

S/I direction on the femoral head. This load is the most basic loading to simulate a pure weight loading on the femoral head. The M/L direction or the positive X direction is simulated at 250 N. While the S/I direction or positive Z direction is simulated at 1350 N. The second loading is a one legged standing with weight loading on the femoral head in the M/L direction, A/P direction and S/I direction. These loadings are 250 N in the M/L direction, 200 N in the A/P direction and 1350 N in the S/I direction. The third loading is the simulation of a dynamic load in which the static loads are increased by doubling the amount of the static loading. The forces of this loading condition are 500 N in the M/L direction, 400 N in the A/P direction and 2700 N in the S/I direction. The final loading condition involves the forces of climbing a stair. These forces are applied on the femoral head and the greater trochanter. For the femoral head, the forces are 500 N in the M/L direction, 150 N in the A/P direction and 2700 N in the S/I direction. For the greater trochanter, the forces are -400 in the M/L direction, 0 N in the A/P direction and -1100 in the S/I direction. These two forces produce a bending moment on the proximal end of the femur. By simulating this load, the bone and gamma nail are tested to the limits. The fourth load is simulated to impart an A/P load of 250 N and an S/I load of 1350 N. This load depicts a standing load with a forward shift in the person's weight from the anterior to posterior. The fifth load is simulated to impart an A/P load of 250 N, M/L load of 200 N and S/I load of 1350 N. This load simulates a person standing on one leg with their weight shifted slightly forward. The final load has an A/P load of 500 N, M/L load of 400 N and S/I load of 2700 N. This load simulates a dynamic load of a person standing on one leg with their weight slightly forward. The load conditions are stated in Figure 9, along with their abbreviations. These loads are simulated various positions of loading on the femoral head and the load transferred through the bone and gamma nail. In this process of the simulation, the constraints are defined. The femurs distal end is relatively stationary during all loading conditions. The base of the femur is constrained to zero movement in all directions. In the model, the distal end of the femur is modeled as a flat surface. The geometry of the femur is irrelevant as long as it is constrained to zero movement thus, providing the reference for all the calculations of the model [16].

Load Condition (X, Y, Z) (N)	Abbreviation
(0, 250, 1350) on femoral head	LC I
(200, 250, 1350) on femoral head	LC II
(250, 0, 1350) on femoral head	LC III
(250, 200, 1350) on femoral head	LC IV
(500, 400, 2700) on femoral head	LC V
(500, 150, 2700) on femoral head (-400, 0, -1100) on greater trochanter	LC VI

Table 1. Load conditions and Abbreviations

The simulations of these loads are used to determine the stresses and deformation of the bone and Gamma III Implant system^{TM}. The Ansys software package offers a full assortment of deformation, strain and stress calculations. The core calculations used during this simulation phase is the total deformation, von Mises Stress and the maximum shear stress.

V. RESULTS

The results of the simulations conducted, will be divided into three categories. These categories are based on the angle of the lag screw. Each section is based on six loading scenarios that are applied to both a gamma nail and bone. In the gamma nail and bone models a complex fracture is added to the femur just below the femoral head, one of the described locations that utilizes this nail. The loading simulates both a static and quasi-static loading with loads that are similar to those felt under a dynamic situation. Each one of the three categories has different distal screw configurations. These distal screw configurations will show an optimal configuration for the loading and the lag screw angle as it is placed into the femoral head. The three data set compared are the total displacement, von Mises stress and the maximum shear stress. From these values, the maximum stress will be determined and ultimately compared to an S-N diagram. A determination as to how long the material will last until fatigue failure, i.e. failure due to excessive loading during a number of cycles, was conducting within this survey.

The loads and the distal screw configuration are the two criteria in which these results are sorted. There are six loads applied to this model, as previously discussed in the modeling section. The distal screw configuration is set into the following configuration: the single static distal screw, the 20 mm between the two distal screws, the 40 mm separation between the two distal screws, the 20 mm between the two distal screws in a dynamization configuration, 40 mm between the two distal screws in a dynamization configuration and the dynamic distal screw.

The 40 mm distal screw configuration is the design improvement that is being proposed within this study, given that the other distal screw configurations are configurations that exist already in the gamma nail. The gamma nail is modeled with the three holes fabricated in the nail to determine the stress level at the voids. By doing this, the model will be useful in determining the practicality of the improvement from a gamma nail perspective.

Each loading condition affects the gamma nail in slightly different ways. For example, a bending movement is introduced in load six and torsional effects are

introduced in loads one and two. These results will show how well the stress is dispersed throughout the system and which element is the limiting factor. However, from past studies the distal screws are shown to be the main limiting factors. The major concern is whether this hold true when the gamma nail is altered slightly and with the introduction of different distal screw configurations.

The following shows the screw arrangement on the charts. It is important to know this information in order to be acquainted with the charts and their meaning.

Screw Configuration	Abbreviation
Single Static Locking Screw	SSL
Two Distal Screws with 20 mm Separation	TSL20
Two Distal Screws with 40 mm Separation	TSL40
Two Screws With Dynamic Locking (reversed) with 20 mm Separation	TDL20R
Two Screws With Dynamic Locking 20 mm Separation	TDL20R
Two Screws With Dynamic Locking 40 mm Separation	TDL40
Single Dynamic Locking	SDL

Table 2. Screw Configuration Abbreviations.

A. 120-DEGREE LAG SCREW

1. Von Mises Stress

120-degree lag screw configuration of the gamma system produced the result shown in the following Figures 34, 35, 36, and 37 for the von Mises stress. The purpose of this formulation is to find the combination that produces the lowest results, therefore minimizing the chance of ductile failure

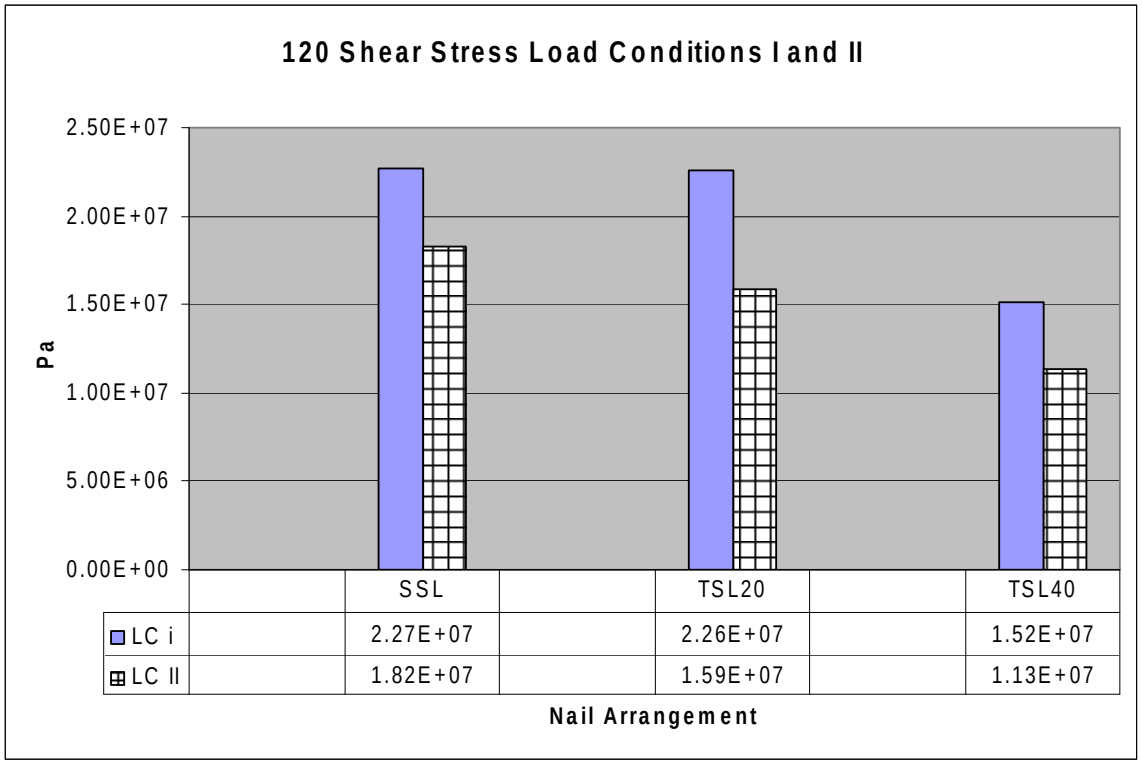

Figure 34. Von Mises Stress for Loads I and II

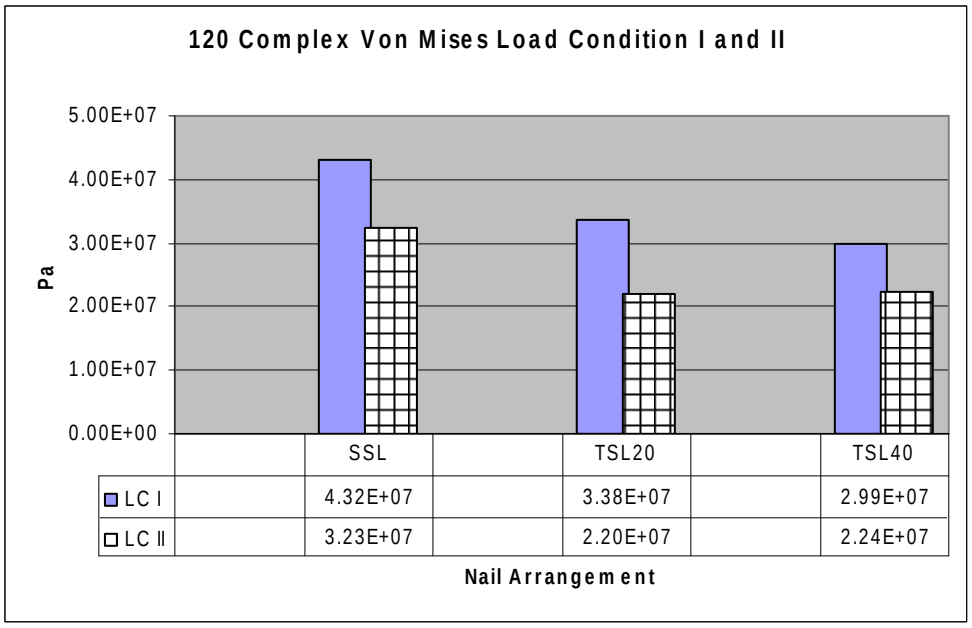

Figure 35. Von Mises Stress With Complex Fracture With Load I and II

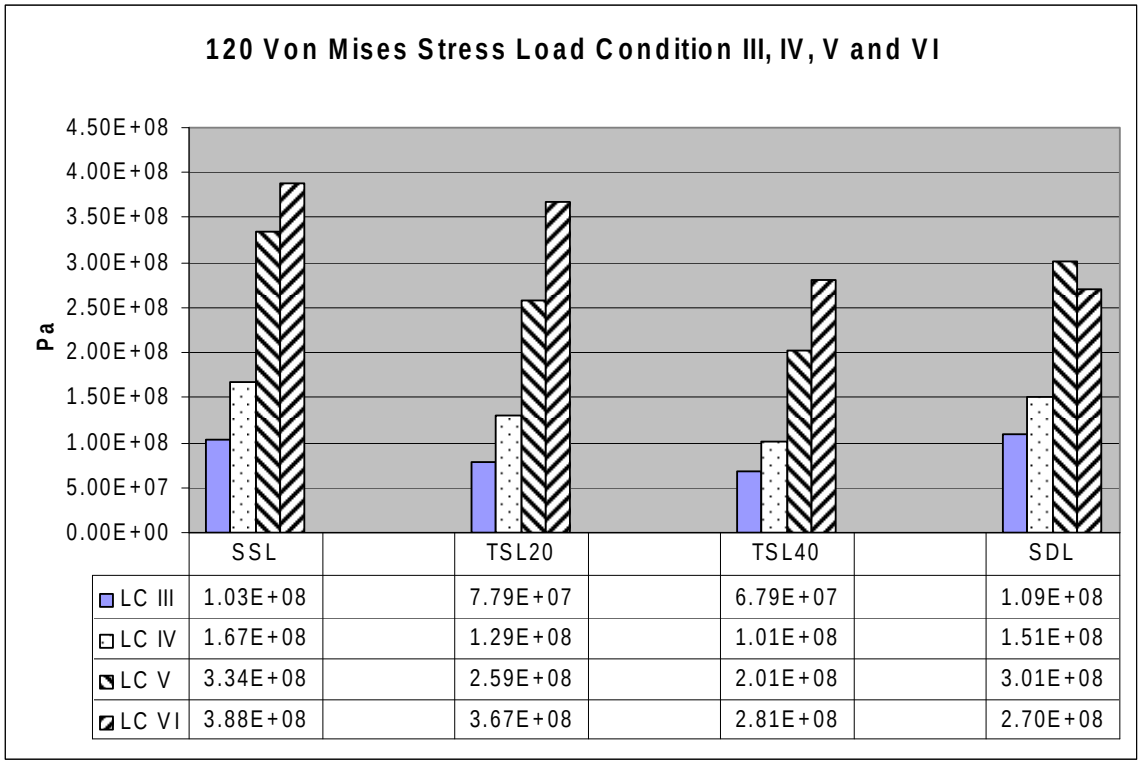

	SSL	TSL20	TSL40	SDL
LC III	1.03E+08	7.79E+07	6.79E+07	1.09E+08
LC IV	1.67E+08	1.29E+08	1.01E+08	1.51E+08
LC V	3.34E+08	2.59E+08	2.01E+08	3.01E+08
LC VI	3.88E+08	3.67E+08	2.81E+08	2.70E+08

Figure 36. Von Mises Stress Of Bone and Nail under Loads III, IV, V and VI

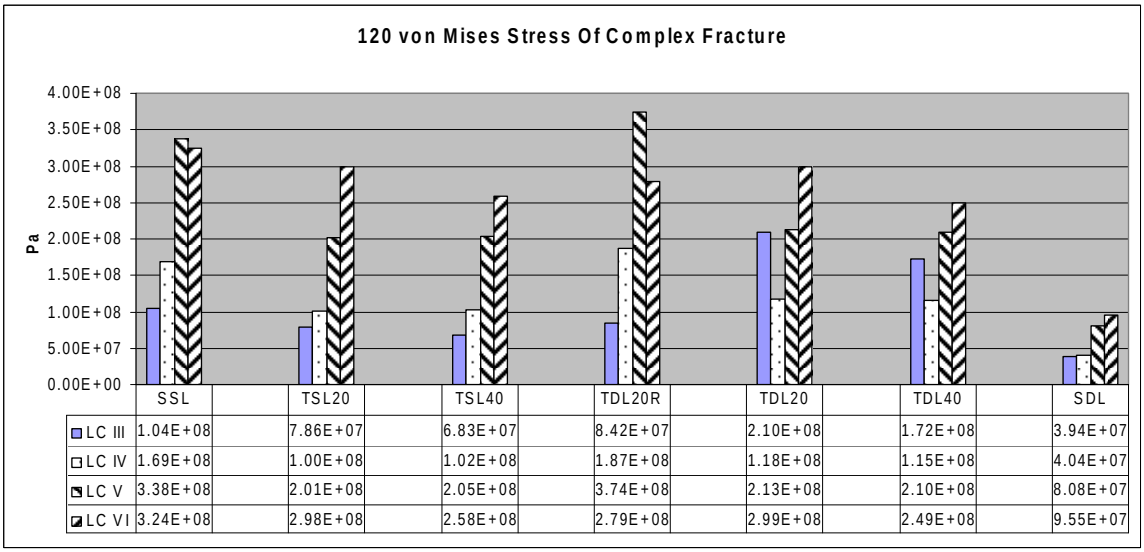

	SSL	TSL20	TSL40	TDL20R	TDL20	TDL40	SDL
LC III	1.04E+08	7.86E+07	6.83E+07	8.42E+07	2.10E+08	1.72E+08	3.94E+07
LC IV	1.69E+08	1.00E+08	1.02E+08	1.87E+08	1.18E+08	1.15E+08	4.04E+07
LC V	3.38E+08	2.01E+08	2.05E+08	3.74E+08	2.13E+08	2.10E+08	8.08E+07
LC VI	3.24E+08	2.98E+08	2.58E+08	2.79E+08	2.99E+08	2.49E+08	9.55E+07

Figure 37. Von Mises Stress for Loads III, IV, V and IV

The figures above show the von Mises stresses for the various distal screw configurations. Starting with Figure 30, the distal screw configuration is a single screw in a static lock, two screws at 20 mm separation in a static lock (TSL20) and two screws at 40 mm separation (TSL40) in a static lock. As seen from the figure, the two screws at a 40 mm separation has the lowest von Mises stress with a value of 2.98e7 Pa in load I and 1.96e7 Pa in Load Case II. These two values are significantly lower than that of the other two-screw configuration in this Figure 34. There is an approximate decrease of 25 percent in stress seen in these load conditions compared to that of the other two distal screws configuration. Looking at the Load Cases I and II; and determining which load is the limiting the complex fracture model, the results demonstrate the favorable distal screw configuration as two screws with 40 mm between the screws. From this argument, the first load is the limiting load in which the two-screw configuration is an improvement by approximately 11 percent. The dynamic screw configuration produced the largest stresses by almost two fold.

In the next series of loadings, the models show note-worthy results. By visual inspection, it is apparent that the models with the distal screw configuration of two-screws with 40 mm (TSL40) between the screws produce the best results, showing the results are lowest in value. These values are an improvement by approximately 13 percent in load case III and 25 percent in load case VI. In this case, the two-screw combination with 40 mm spacing is an improvement in all load cases. Models depicting the bone and the complex fractured bone show that the two-screw combination of 20 mm and 40 mm are almost exacting except in the case of the quasi-static condition modeled in load case VI. In this case, the two screws with 40 mm separation is an improvement by 14 percent. In looking at the dynamic locking combination of the distal screws, the two screws with the 40 mm spacing proved to produce better results in a dynamic locking.

2. Shear Stress

Shear stress is the stress that is applied to the parallel or tangential to a face of a material as opposed to the normal [18]. Therefore, the maximum shear stress is the maximum stress applied to the parallel or tangential before failure occurs. These results

are noteworthy given the depiction of the loading conditions; the two distal screw with 40 mm distance between them is the most efficient configuration, as seen in the following Figures 38, 39, 40, and 41.

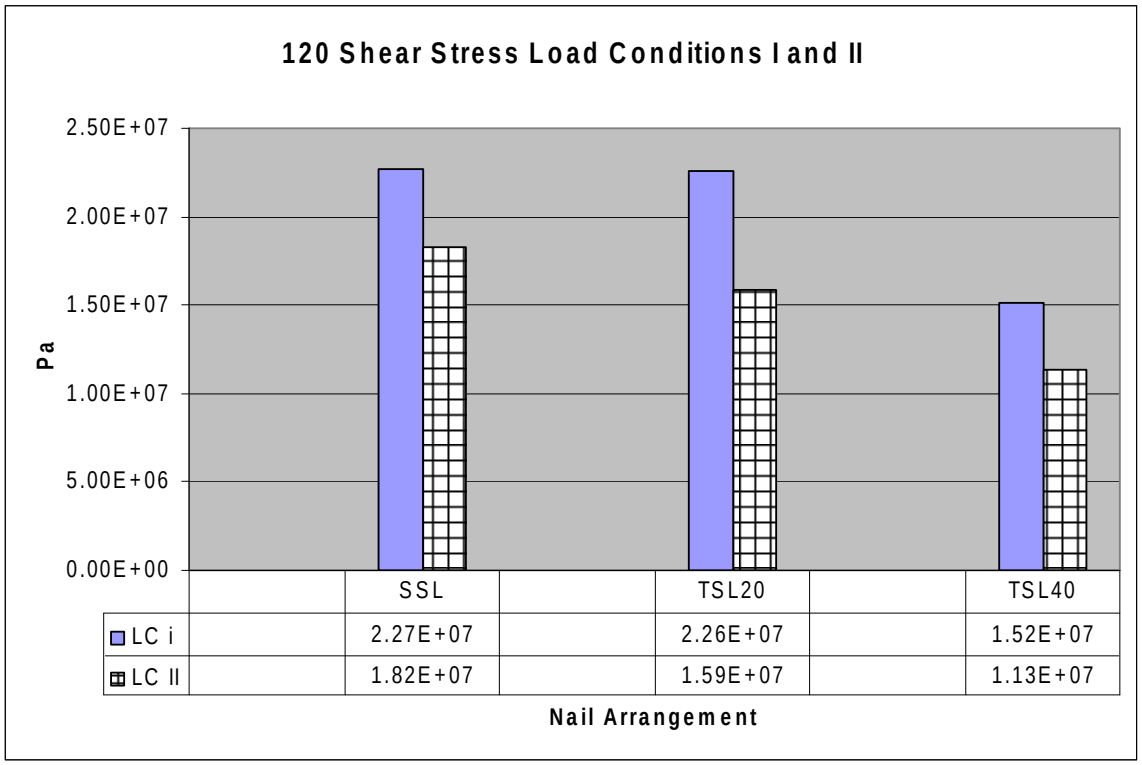

Figure 38. Shear Stress For Load condition I and II, No Fracture

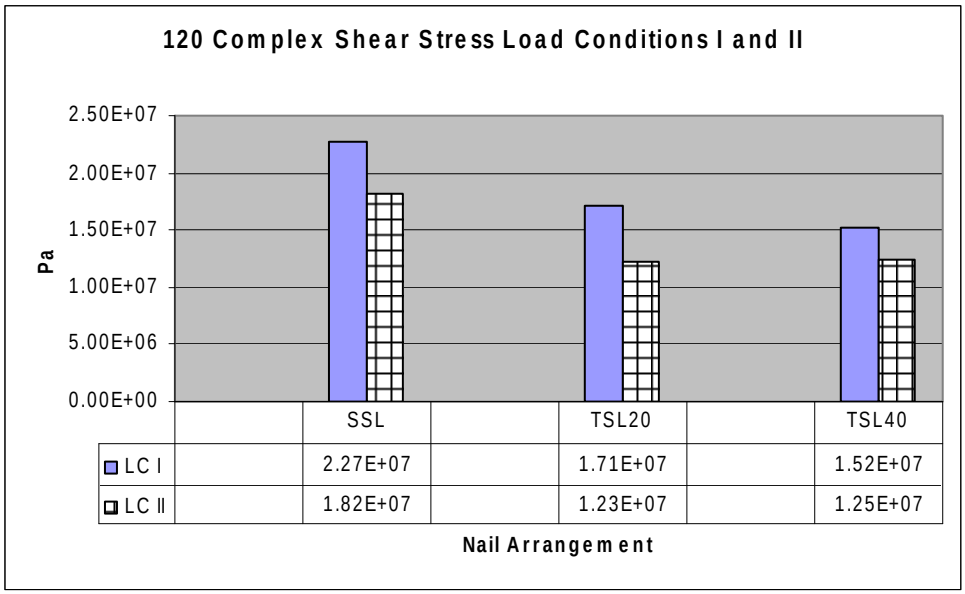

Figure 39. Shear Stress For Load Condition I and II with Fracture

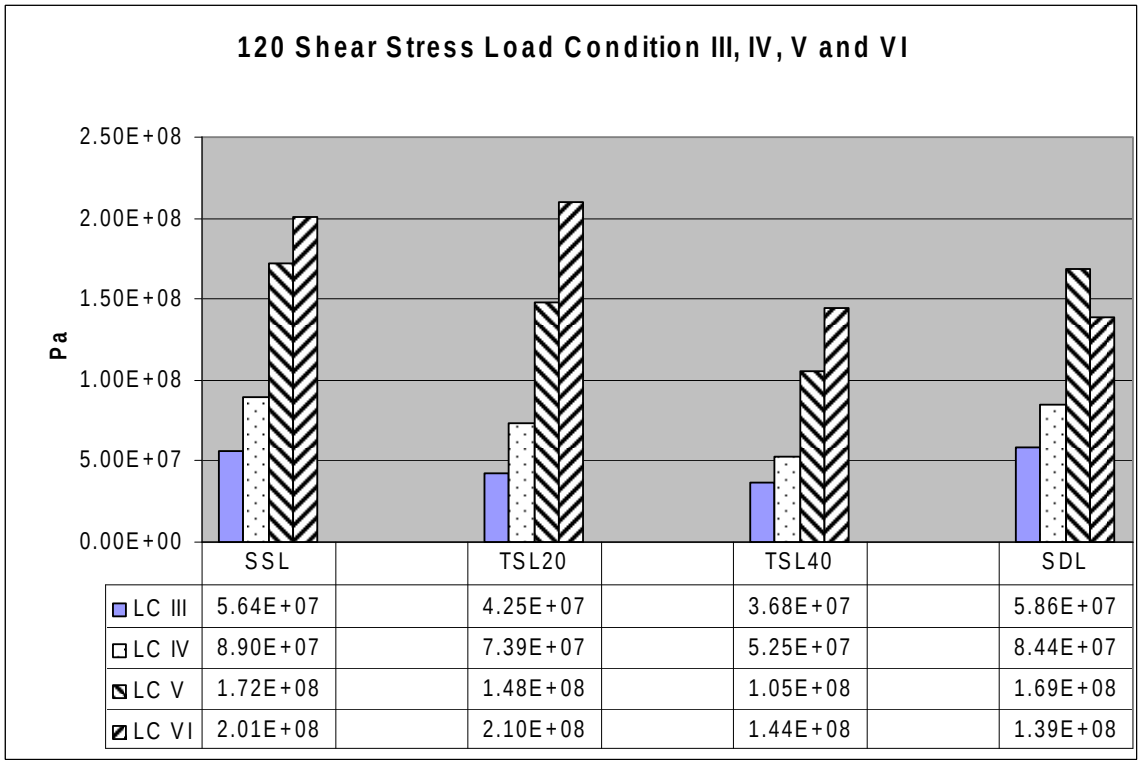

Figure 40. Shear Stress For Load Condition III, IV, V and VI, No Fracture

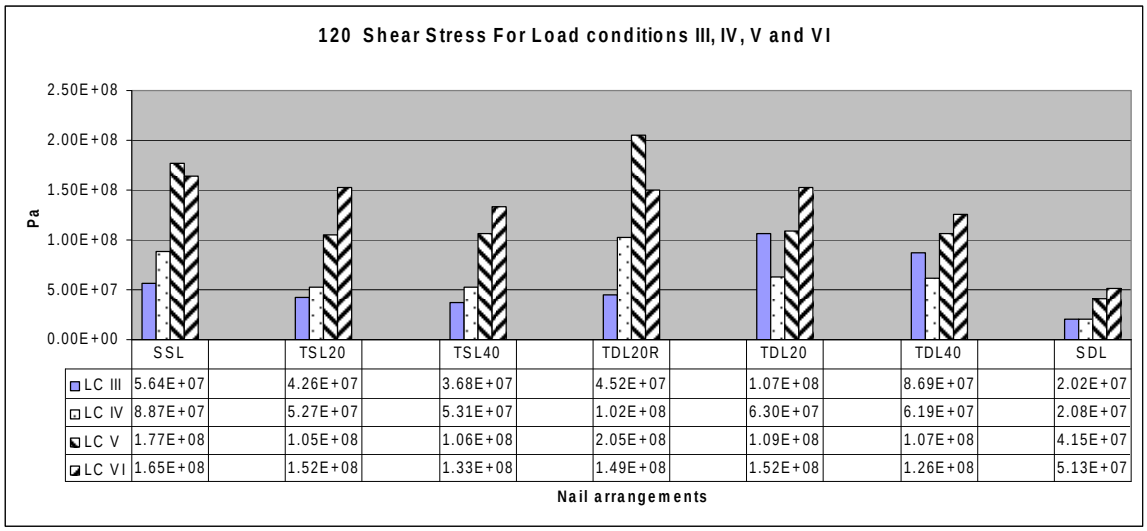

Figure 41. Shear Stress For Load Condition III, IV, V and VI, Fracture

The shear stress follows congruently with the von Mises stress, in that the same phenomenon occurs. While the most limiting distal screw combinations are the single static distal locking screw and reversed dynamic screw combination, the shear stress illustrates that the two-distal screws with 40 mm separation (TSL40) is the furthest away from the ultimate tensile strength.

B. 125-DEGREE LAG SCREW

1. Von Mises

The 125-degree lag screw is the next to be evaluated, as seen in Figures 42, 43, 44, and 45. The purpose of this formulation is to find the combination that produces the lowest results consequently minimizing the chance of ductile failure. The results indicate that the two screw combinations produce the best results, meaning these combinations have lower stress values thus increasing their lifetime use and resistance to ductile failure.

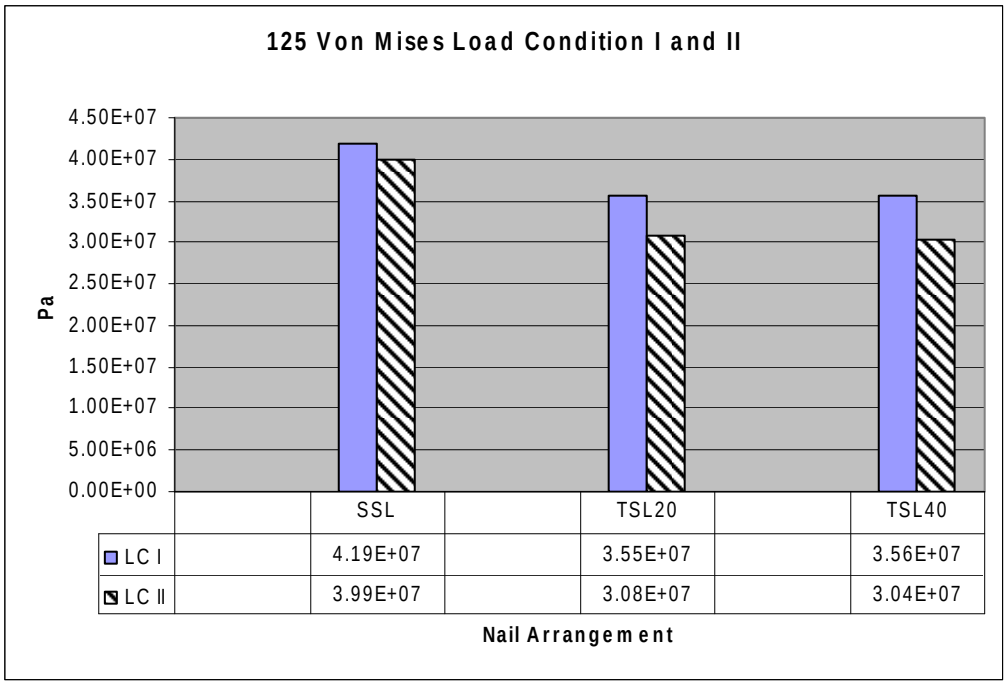

Figure 42. 125 Degree Lag Screw Under Load Condition I and II, No Fracture

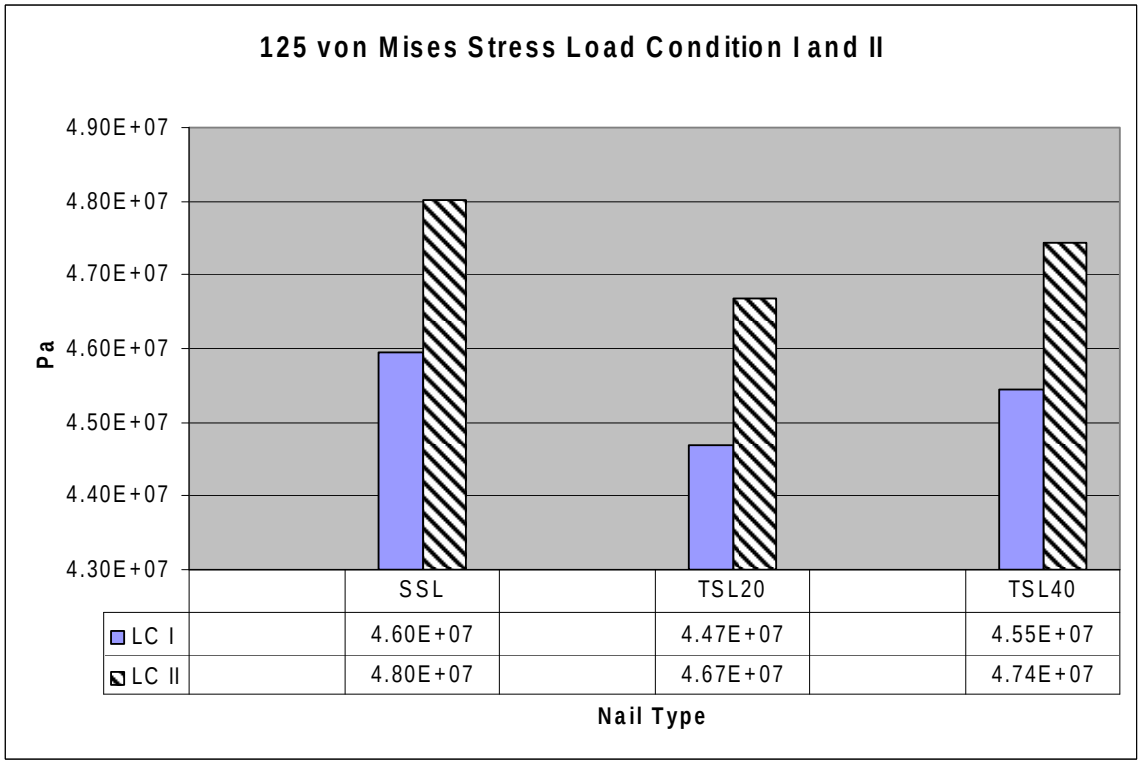

Figure 43. Degree Lag Screw Under Load Condition I and II, With Fracture

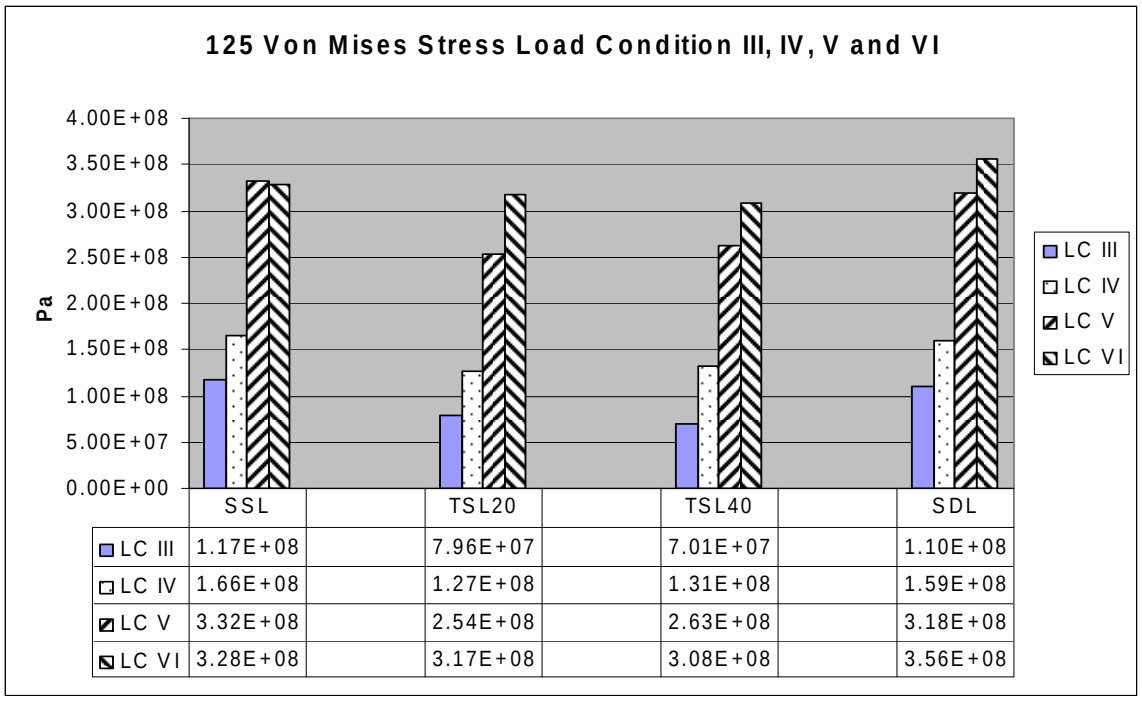

	SSL	TSL20	TSL40	SDL
LC III	1.17E+08	7.96E+07	7.01E+07	1.10E+08
LC IV	1.66E+08	1.27E+08	1.31E+08	1.59E+08
LC V	3.32E+08	2.54E+08	2.63E+08	3.18E+08
LC VI	3.28E+08	3.17E+08	3.08E+08	3.56E+08

Figure 44. Degree Lag Screw Under Load Condition III, IV, V and VI, No Fracture

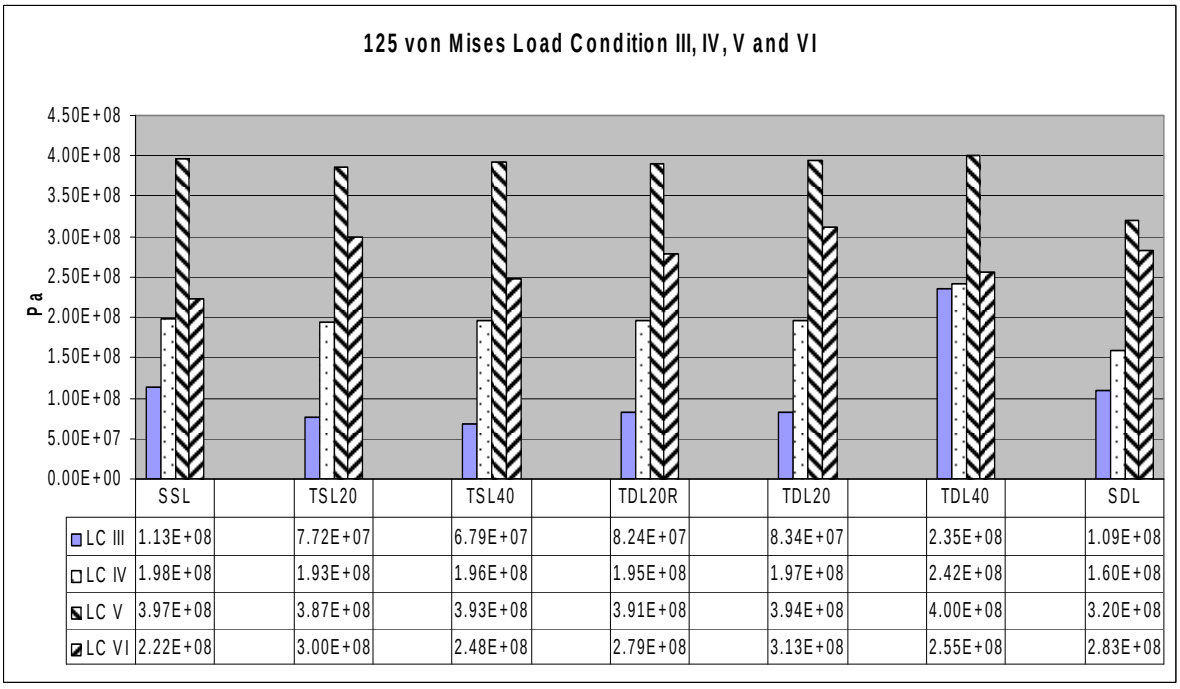

	SSL	TSL20	TSL40	TDL20R	TDL20	TDL40	SDL
LC III	1.13E+08	7.72E+07	6.79E+07	8.24E+07	8.34E+07	2.35E+08	1.09E+08
LC IV	1.98E+08	1.93E+08	1.96E+08	1.95E+08	1.97E+08	2.42E+08	1.60E+08
LC V	3.97E+08	3.87E+08	3.93E+08	3.91E+08	3.94E+08	4.00E+08	3.20E+08
LC VI	2.22E+08	3.00E+08	2.48E+08	2.79E+08	3.13E+08	2.55E+08	2.83E+08

Figure 45. Degree Lag Screw Under Load Condition III, IV, V and VI, With Fracture

The results of the von Mises calculations demonstrate the diversity of the results. The results are not definitive as to which distal screw combination yields the best results. This is seen in Figure 45, the graphs depicting the load conditions III thru VI with a fractured bone. When reviewing these results, both the two screw 20 mm and two screw 40 mm are similar in their maximum stress values. Ultimately, the results should be viewed by which combination brings the Gamma III Implant system^{TM} to its maximum tensile strength. The best results in load conditions IV and V are produced with the two distal screw with a 40 mm distance (TSL40). These both have the same loading components but the forces in load condition V are double that of load condition IV. In addition, the distal screw combination with 20 mm (TSL20) separation produced the best results under load conditions II and I with a fracture in the bone, by about 2 percent, while the screw combination with two screws and 40 mm between the screws produce the best results in load condition III and VI. The cracked bone models under load conditions III, IV, V and VI seem to be the limiting set of models. In particular, the load condition V for the fractured model, is a dynamic load simulation in a quasi-static model. Under this load condition, all models simulated are within 4 percent of the critical stress, except for the single dynamic locking screw (SDL). Therefore, this is the critical loading of these models and produces consistent forces that will increase the likelihood of fatigue failure.

2. Shear Stress

The maximum shear stress of this model shows the largest of shear stress acting in any direction on any plane in the model. Therefore, the results in the model will show areas of possible ductile failure. In the following Figures 46, 47, 48, and 49, the maximum shear stress for the 125-degree lag screw and various distal screw combinations is determined.

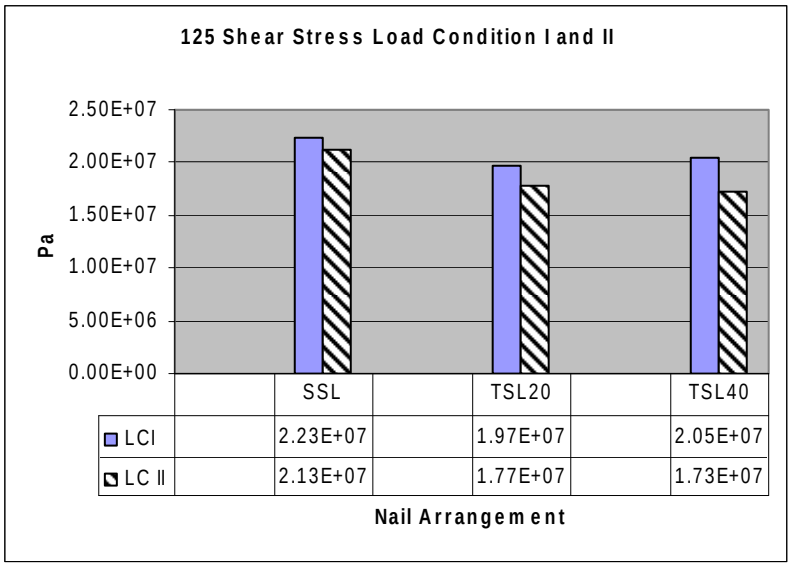

Figure 46. Maximum Shear Stress For Load Condition I and II, No Fracture

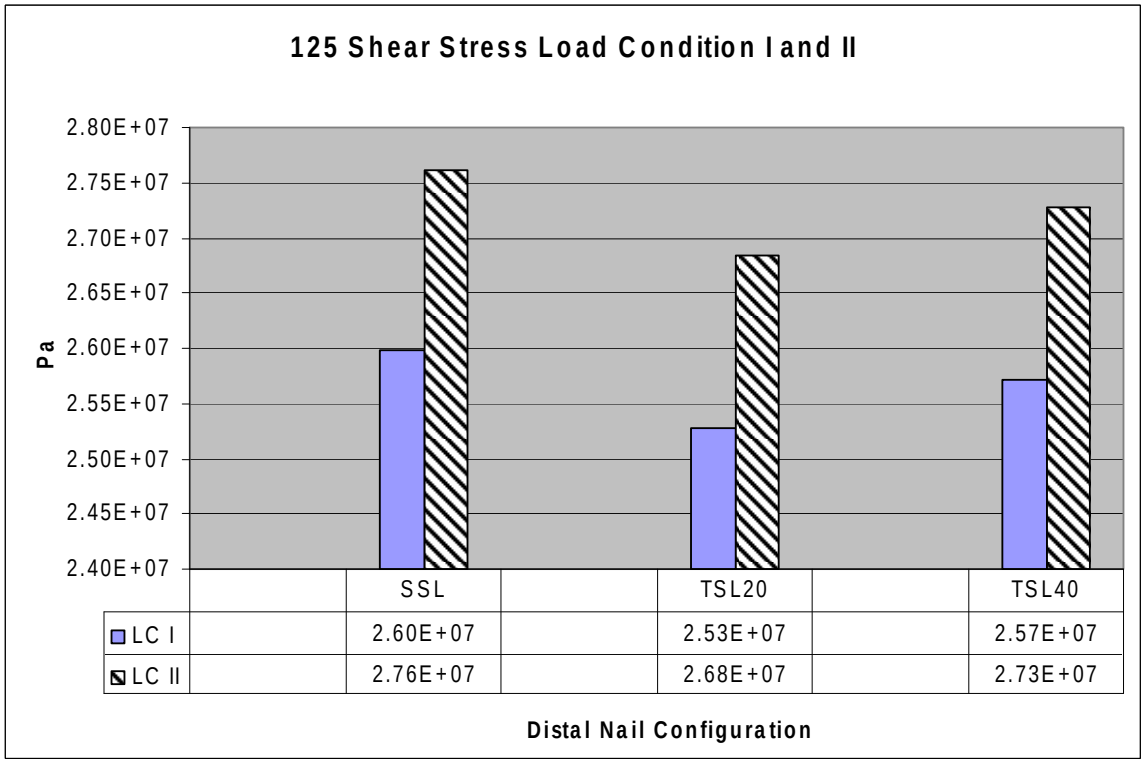

Figure 47. Maximum Shear Stress For Load Condition I and II, With A Fracture

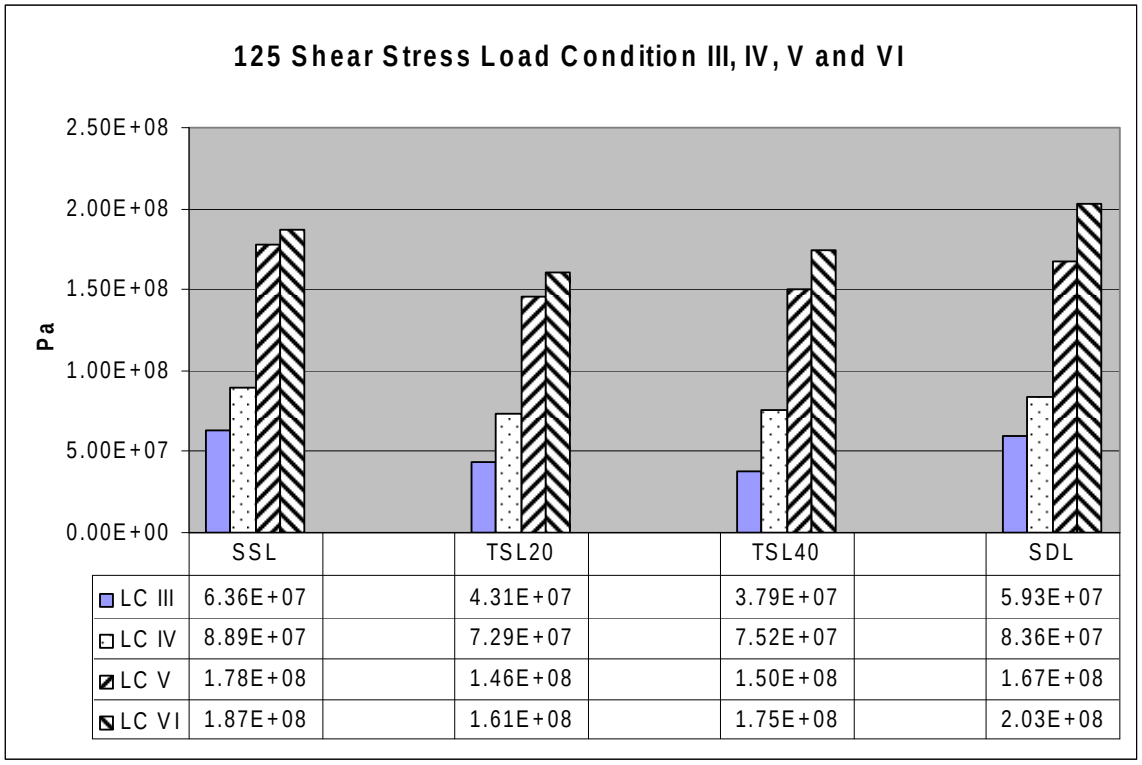

	SSL	TSL20	TSL40	SDL
LC III	6.36E+07	4.31E+07	3.79E+07	5.93E+07
LC IV	8.89E+07	7.29E+07	7.52E+07	8.36E+07
LC V	1.78E+08	1.46E+08	1.50E+08	1.67E+08
LC VI	1.87E+08	1.61E+08	1.75E+08	2.03E+08

Figure 48. Maximum Shear Stress For Load Condition III, IV, V and VI, No Fracture

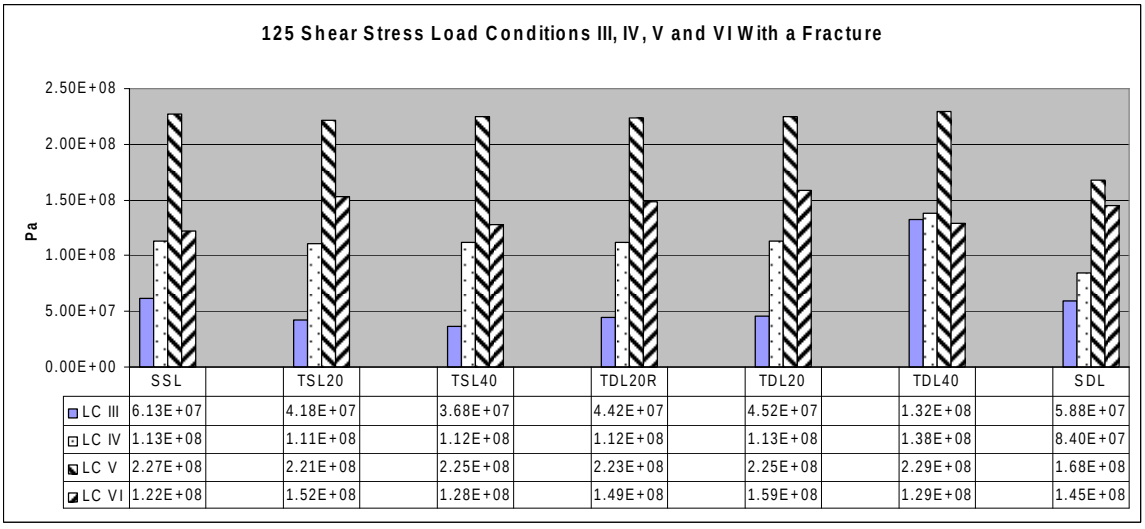

	SSL	TSL20	TSL40	TDL20R	TDL20	TDL40	SDL
LC III	6.13E+07	4.18E+07	3.68E+07	4.42E+07	4.52E+07	1.32E+08	5.88E+07
LC IV	1.13E+08	1.11E+08	1.12E+08	1.12E+08	1.13E+08	1.38E+08	8.40E+07
LC V	2.27E+08	2.21E+08	2.25E+08	2.23E+08	2.25E+08	2.29E+08	1.68E+08
LC VI	1.22E+08	1.52E+08	1.28E+08	1.49E+08	1.59E+08	1.29E+08	1.45E+08

Figure 49. Maximum Shear Stress For Load Condition III, IV, V and VI, With A Fracture

By breaking down the loading of the gamma nail with a lag screw at 125 degrees, it is easy to determine the results are uniform across the distal configurations. The distal combination that produce the lowest results overall was the two screw combination with 20 mm in between the screws. This combination produced the lowest values in most loaded condition except the following: load condition II in Figure 47, load condition III and load condition VI in Figures 48 and 49. In these instances, the distal screw combination with two screws separated by 40 mm was the model with lower stress. In addition to just the raw numerical data, Figure 50 and 51 shows the areas of high stress concentration. These areas are mostly located in the distal screws as seen in the figures below. The results shown indicate that load condition V is the critical load, which confirms the results of the von Mises Stress data. In addition, the consideration of which screw arrangement is best suited for dynamic locking seems to the distal screw configuration with 20 mm separation. It has yielded results that are lower than the other dynamic configuration in the three of the four loads, which it was subjected.

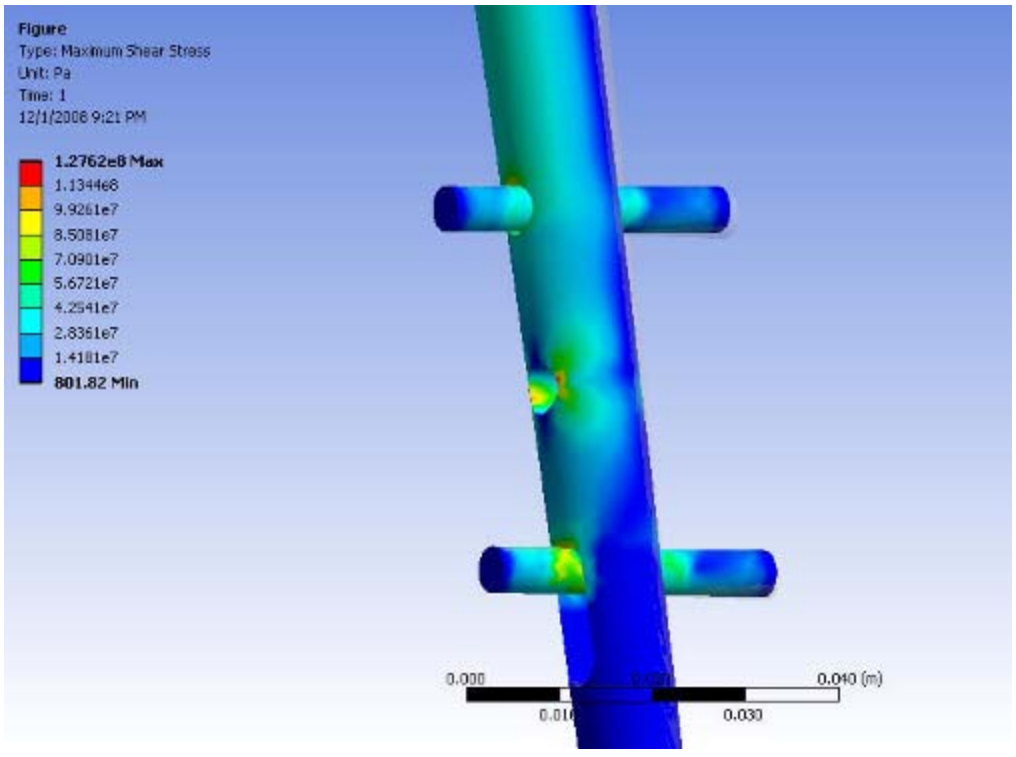

Figure 50. Distal Screw Configuration With 40 mm Load VI

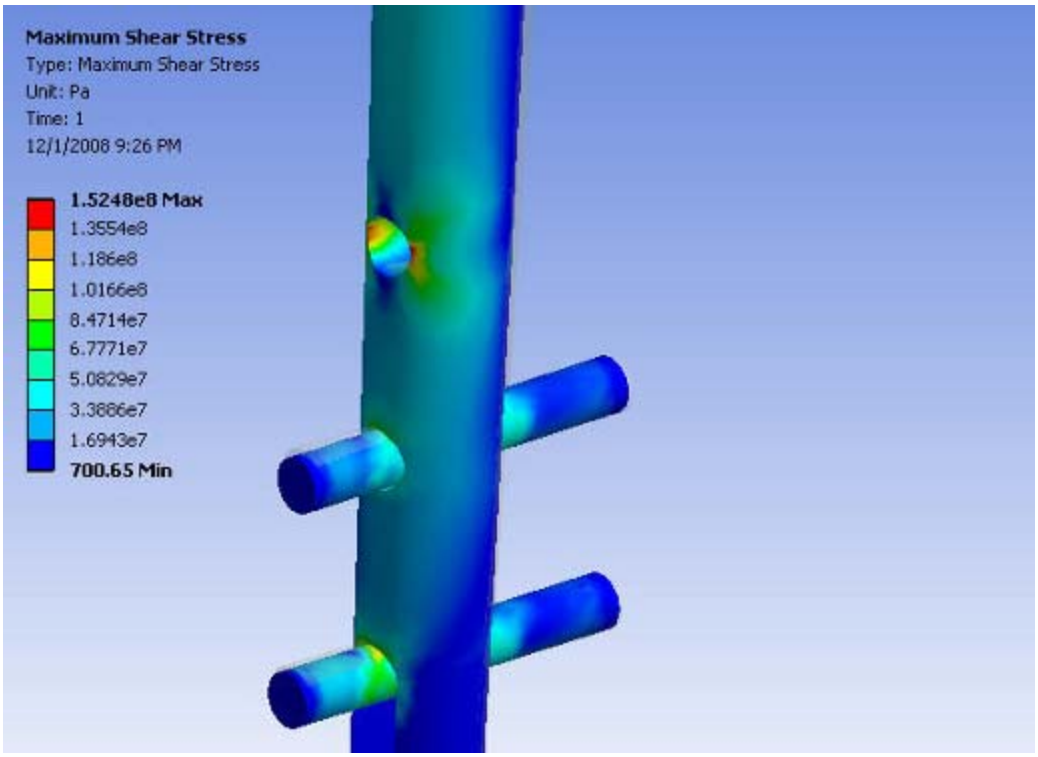

Figure 51. Distal Screw Configuration With 20 mm Load VI

C. 130-DEGREE LAG SCREW

The final lag angle modeled and simulated is the 130-degree lag screw. Being the final angle to model, this angle is relatively common in the procedure. By performing this model, a complete study of the Gamma III Implant system™ is conducted, producing results useful to orthopedic surgeon's initial surveys.

1. Von Mises

The 130-degree lag screw is the results to evaluate before determining a conclusion for the parametric study. These results will provide a well-rounded scenario for surgeons to use on patients to lower stress concentrations in the Gamma III Implant system™. By evaluating these results, it is apparent that the distal screw combination of two screws with a separation of 40 mm yields the best results. This can be seen in the following Figures 52, 53, 54 and 55.

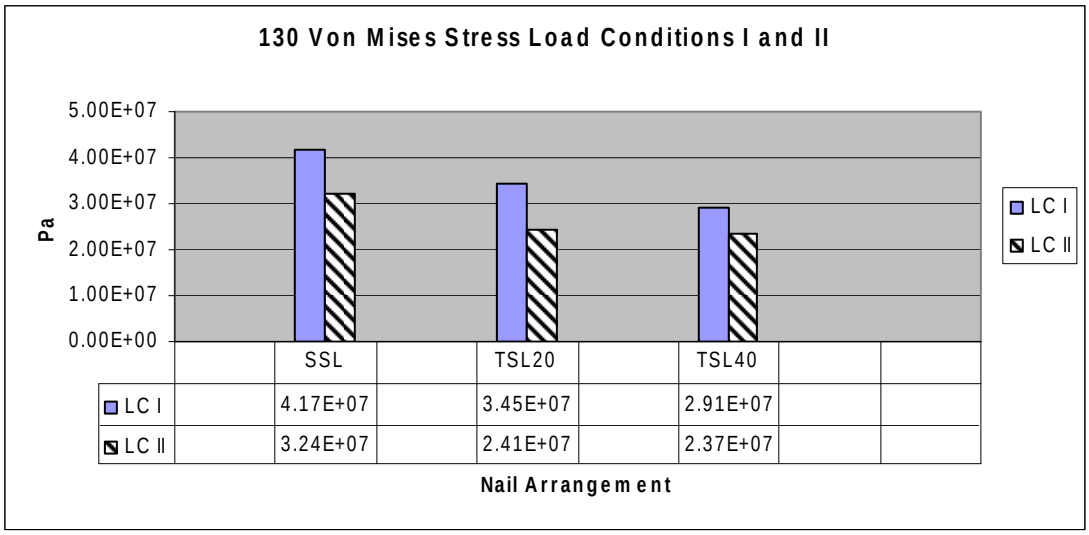

Figure 52. Von Mises Stress Load Conditions I and II, No Fracture

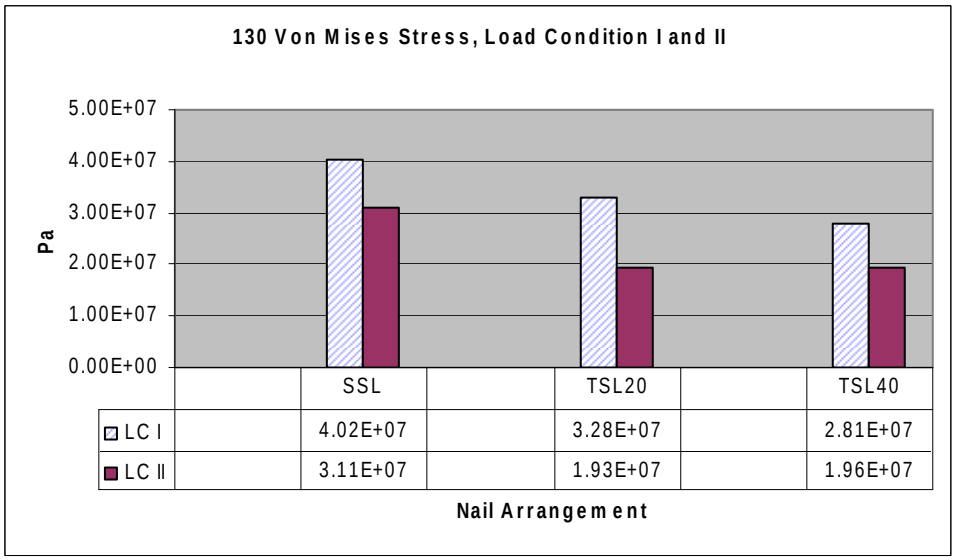

Figure 53. Load Condition I and II, With Fracture

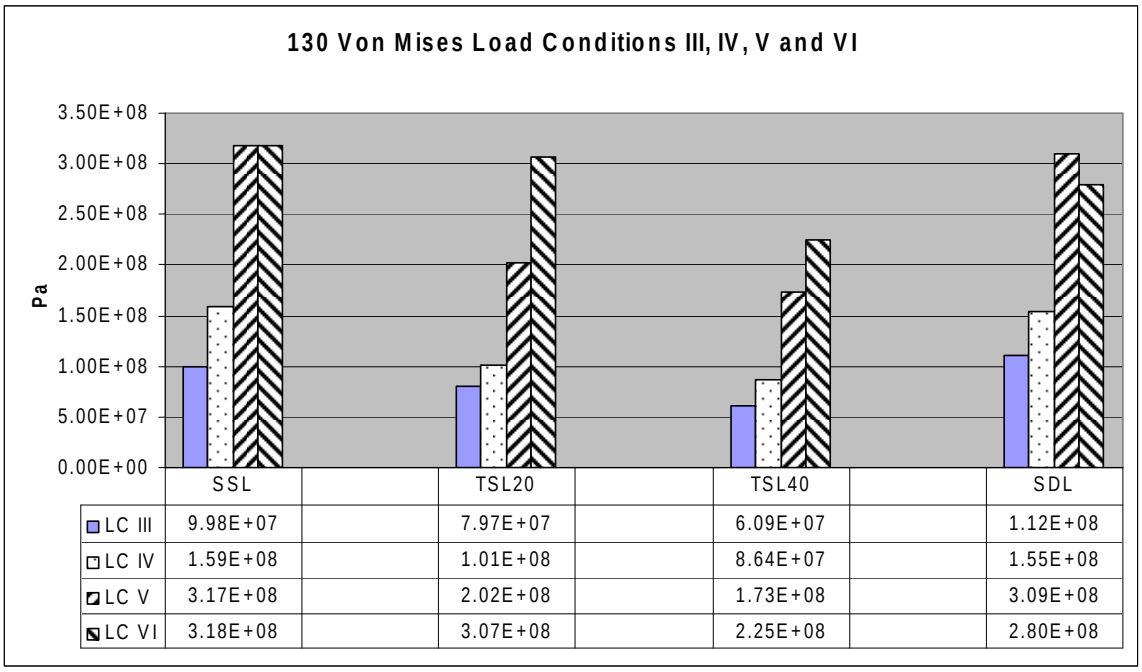

	SSL	TSL20	TSL40	SDL
LC III	9.98E+07	7.97E+07	6.09E+07	1.12E+08
LC IV	1.59E+08	1.01E+08	8.64E+07	1.55E+08
LC V	3.17E+08	2.02E+08	1.73E+08	3.09E+08
LC VI	3.18E+08	3.07E+08	2.25E+08	2.80E+08

Figure 54. Load Conditions III, IV, V and VI, No Fracture

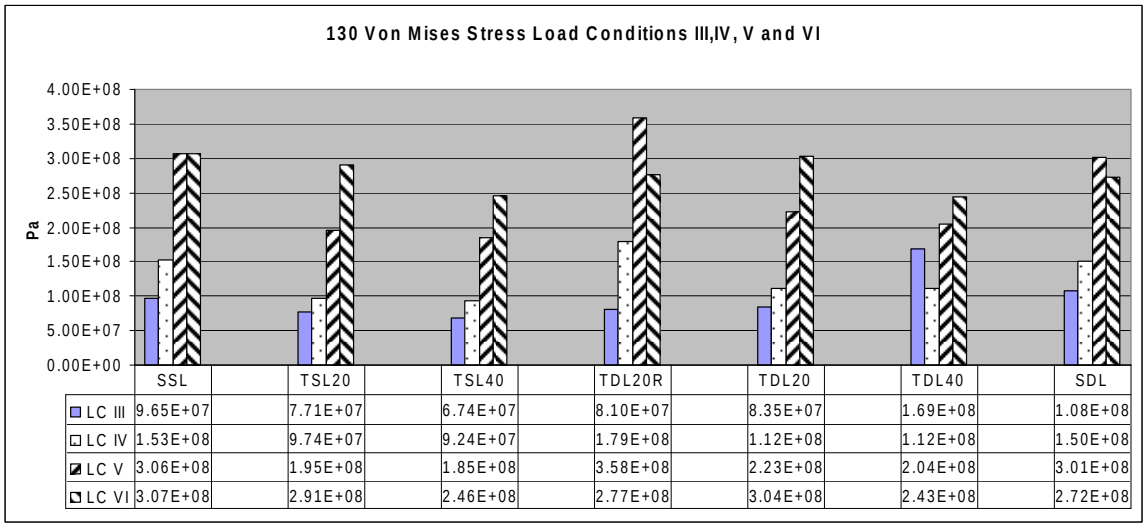

	SSL	TSL20	TSL40	TDL20R	TDL20	TDL40	SDL
LC III	9.65E+07	7.71E+07	6.74E+07	8.10E+07	8.35E+07	1.69E+08	1.08E+08
LC IV	1.53E+08	9.74E+07	9.24E+07	1.79E+08	1.12E+08	1.12E+08	1.50E+08
LC V	3.06E+08	1.95E+08	1.85E+08	3.58E+08	2.23E+08	2.04E+08	3.01E+08
LC VI	3.07E+08	2.91E+08	2.46E+08	2.77E+08	3.04E+08	2.43E+08	2.72E+08

Figure 55. Load Conditions III, IV, V and VI, With Fracture

Since the distal screw configuration, with two screws and 40 mm in a static lock between, is determined to be the best distal screw combination in all the loading scenarios, the next tasks is to determine the worst-case scenario and the critical stress for

the 130-degree group. In reviewing the data from the computational analysis, a trial run was performed by moving the dynamic locking hole to the proximal end of the distal locking screws. This analysis demonstrated that a critical load could be found using load condition V. However, the worst-case scenario is single static screw with a fractured bone under load conditions V and VI. This was also true for the model with no fracture. When looking at the dynamic locking configuration, the distal screw configuration with a 40 mm gap proved to be a better design than that of the model with a 20 mm gap, by at least 9 percent. The advantage for using this distal screw arrangement is that the static distal screw can be removed and allow compression at the fracture due to the dynamic screw which increases bone healing. While reviewing the results from the dynamization lock of the gamma nail with one screw, the von Mises stress will increase from the value with the two screws with a 40 mm gap. The increase is a margin of 11 percent. In the case of a screw arrangement with a 20 mm spacing, the value will decrease by a margin of 11 percent.

The results that yielded the highest stress concentrations were determined to be the critical load. In the case of the 130-degree lag screw, the limiting values were produced from the single static locking screw. These values were approximately, 306 (LC V) and 307(LC VI) MPa. The next limiting value is the two distal screw combination with 20 mm (TDL20) in a dynamic locking configuration. The determination of these loads can be directly related to the reliability of the gamma nail in long-term use.

2. Shear Stress

The shear stress of the 130-degree lag screw shows the areas of possible ductile failure if the maximum critical stress is exceeded. Using this information helps the surgeons determine proper distal screw location. Using the following figures, it can be determined which screw combination produces the lowest shear stress value.

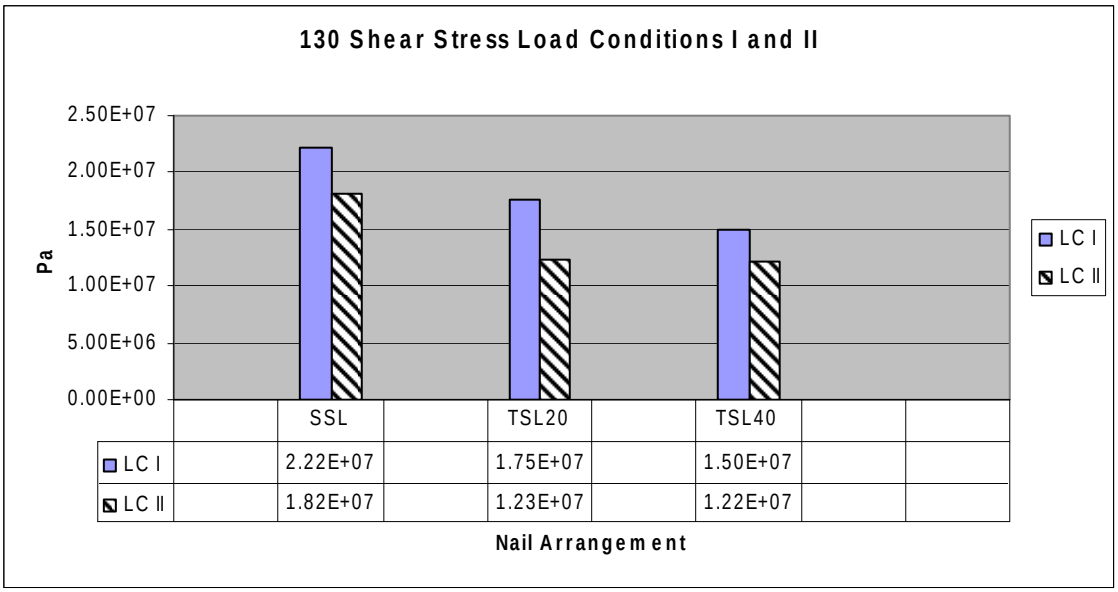

Figure 56. Shear Stress Values from Load Conditions I and II, No Fracture

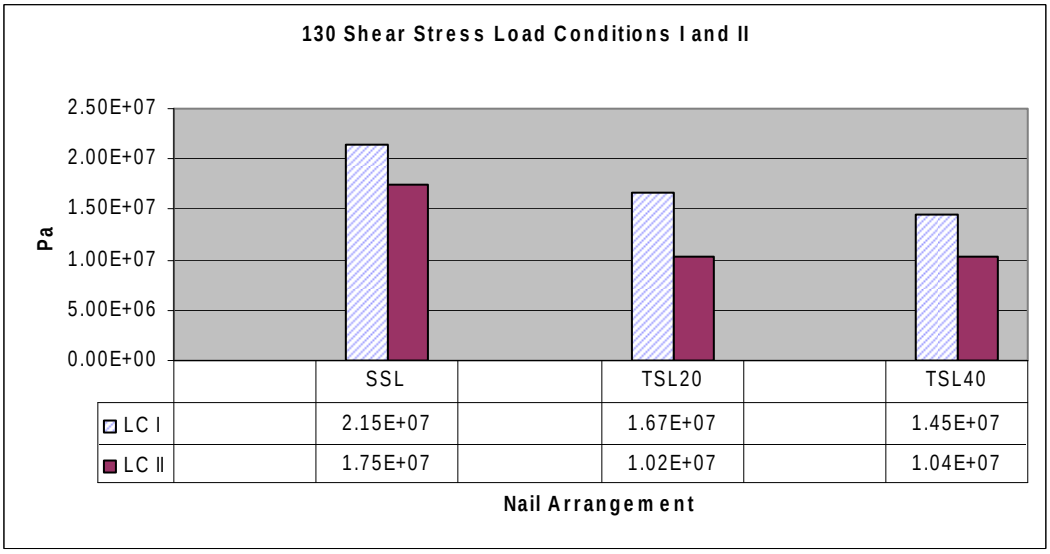

Figure 57. Shear Stress Values From Load Conditions I and II, With A Fracture

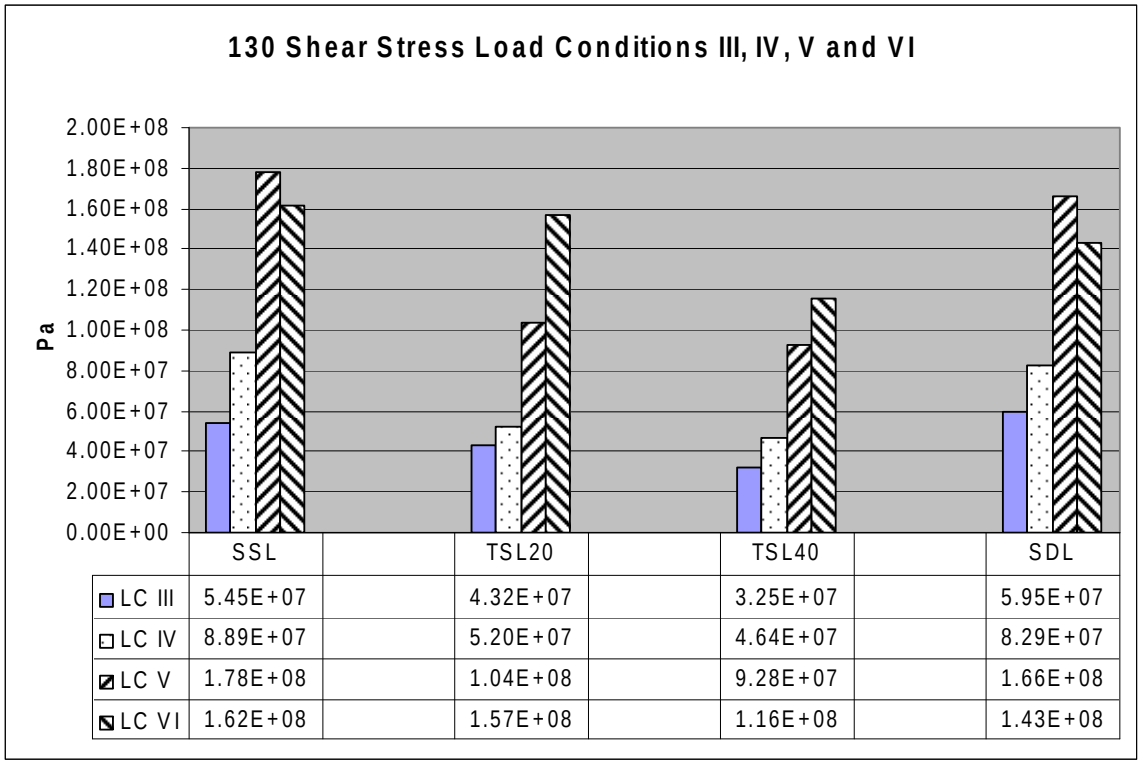

	SSL	TSL20	TSL40	SDL
LC III	5.45E+07	4.32E+07	3.25E+07	5.95E+07
LC IV	8.89E+07	5.20E+07	4.64E+07	8.29E+07
LC V	1.78E+08	1.04E+08	9.28E+07	1.66E+08
LC VI	1.62E+08	1.57E+08	1.16E+08	1.43E+08

Figure 58. Shear Stress From Load Conditions III, IV, V and VI, No Fracture

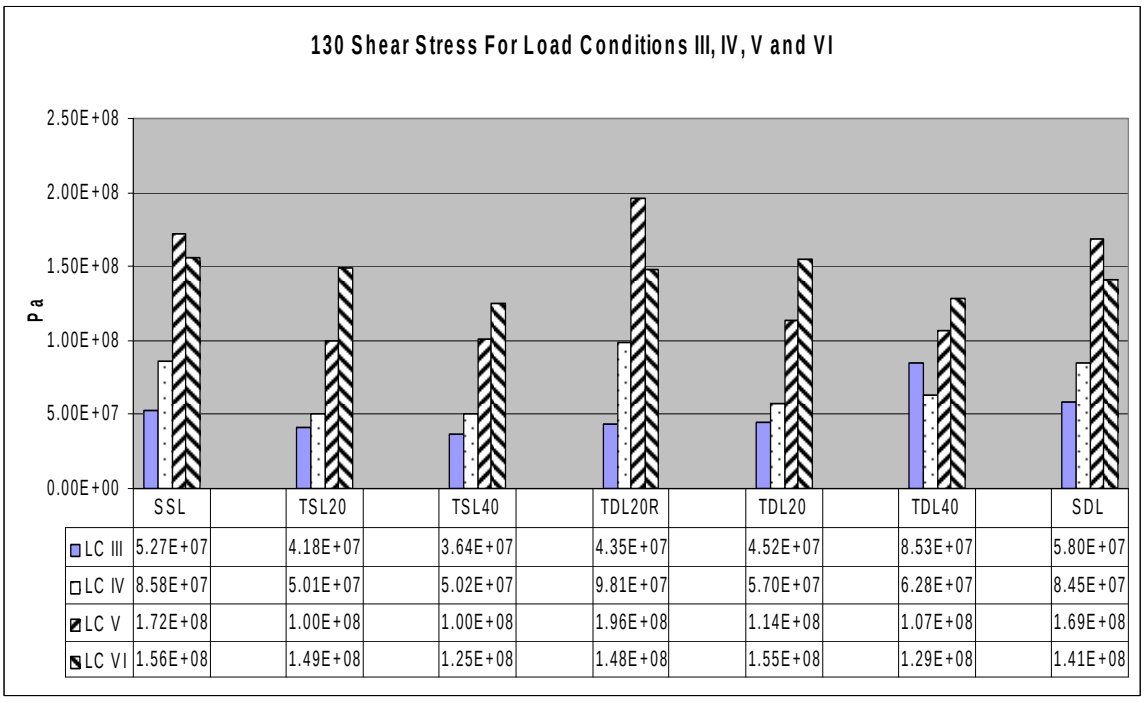

	SSL	TSL20	TSL40	TDL20R	TDL20	TDL40	SDL
LC III	5.27E+07	4.18E+07	3.64E+07	4.35E+07	4.52E+07	8.53E+07	5.80E+07
LC IV	8.58E+07	5.01E+07	5.02E+07	9.81E+07	5.70E+07	6.28E+07	8.45E+07
LC V	1.72E+08	1.00E+08	1.00E+08	1.96E+08	1.14E+08	1.07E+08	1.69E+08
LC VI	1.56E+08	1.49E+08	1.25E+08	1.48E+08	1.55E+08	1.29E+08	1.41E+08

Figure 59. Shear Stress From Load Conditions III, IV, V and VI, With A Fracture

The shear stress models reflect those of the von Mises values. These models show that the maximum shear stress is generally located in the distal screws. The following figures illustrate that some maximum shear stress areas are located in the void hole of the gamma nail. Visual results exemplify the shear stress concentration that occurs in distal screws and the holes.

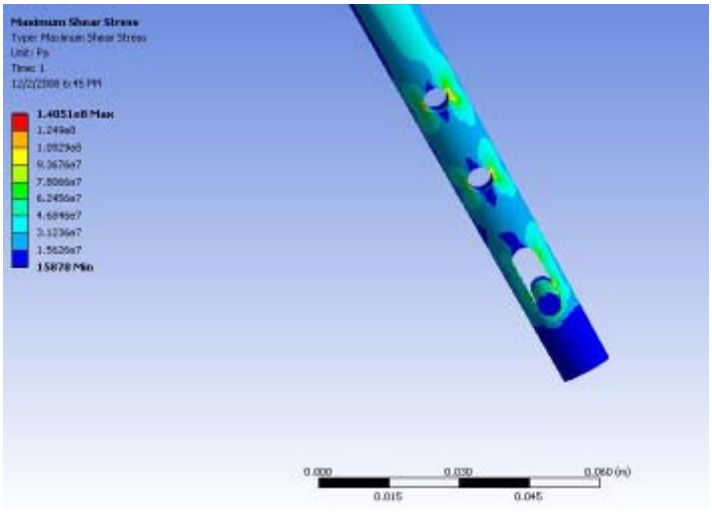

Figure 60. Example Of Maximum Shear Stress in Distal Screw Area

As a result, knowing where the maximum shear stress is located makes it possible to reduce or minimize areas of concern. The maximum shear stress also coincides with the maximum von Mises stress of models with like distal screw configuration.

THIS PAGE INTENTIONALLY LEFT BLANK

VI. CONCLUSION

A parametric study of the Gamma III Implant system^{TM} is a study to improve the link between engineering, medical industry and patient benefits. By conducting this study and trying to improve the current implant system, a benefit can be seen by surgeons and patients. By improving the design in a way that does not change the operational procedure, the minimal invasiveness of the operation is maintained. Improvig the stability of the fracture site and preventing mechanical failure of the device should decrease healing time and reduce the need for future surgeries. Quicker healing time with the decrease chances of returning to the operating room should reduce morbidity and mortality in elderly individuals after sustaining a proximal femur fracture.

The parametric study was conducted by means of implementing the improved gamma nail. As seen in Figures 60, it is evident that the addition of the third distal hole does not lower the integrity of the gamma nail. Distal holes of the gamma nail, in a single screw static configuration, show high stress concentrations in the distal screw hole. Consequently, the addition of an additional distal hole does not impede the integrity of the nail.

Resistance to fatigue failure is an important concern associated with metals placed under cycle stress. In reviewing the works of Prevey and Jayaraman, a variance in the S-N diagram for this titanium alloy, in the case of Ti-6 Al-4 V, is dependent on the location of crack initiation. The S-N diagram displays the applied stress of the material decreases as the number of cycle's increases. If the number of cycles before failure is increased, subsequently the model is improved. If the failure first occurs in the internal structure of the metal, then the S-N diagram is shifted to lower stress limits. As noted in the works of Prevey and Jayaraman, the fatigue failure of the material is below 400 MPa at 10^7 cycles. As a result of this work, there appears to be a linear drop in the fatigue failure to approximately 325 MPa at 10^8 cycles. Using this approximation in the S-N diagram, the determination of which distal-screw configuration should be used justified [19].

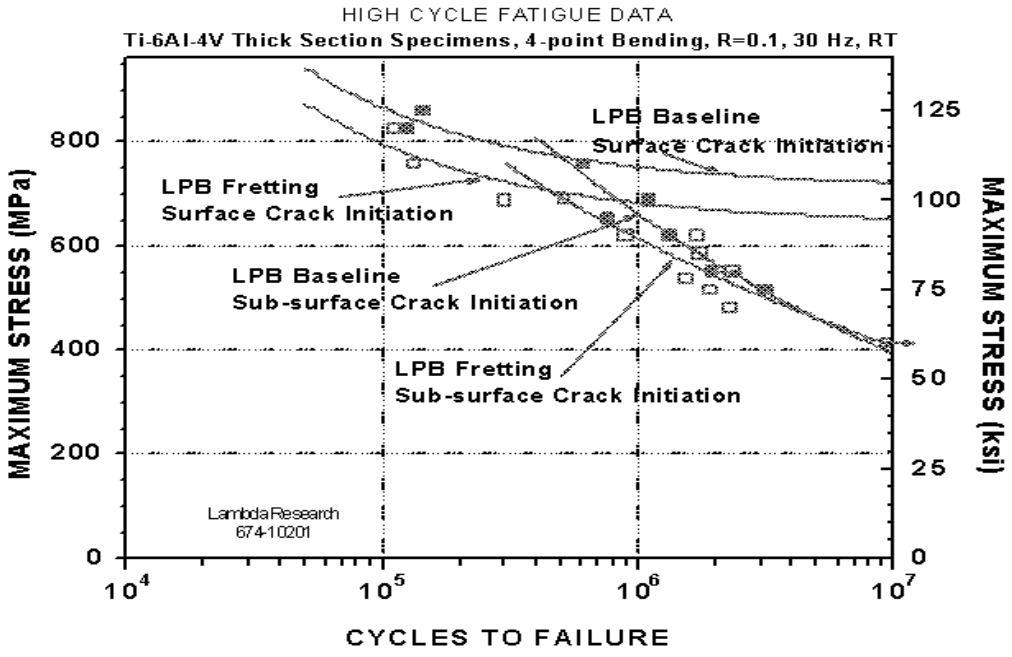

Figure 61. S-N Diagram for Ti-6 Al- 4 V [19]

After conducting the parametric study of the Gamma III Implant system™, results justify the lag screw to distal screw combination. The 120-degree lag screw combination yielded results that reinforced the use of two distal screws with 40 mm between. This is an improvement over the current design in which the von Mises stress and shear stress were decreased by approximately 25 percent in the dynamic locking configuration. In interpreting the results of Prevey and Jayaraman, an increase in the order of magnitude of fatigue failure from approximately 10^8 to approximately 10^9 cycles was seen. These results support the hypothesis that the gamma nail will be cycled further from its failure limits. In addition, by decreasing the stress imposed on the gamma nail in this configuration, the unpredictable stress that occurs from accidents ought to be lowered.

In the 120-degree designs, it is crucial to determine which of the dynamic locking configurations should be chosen. The dynamic locking setup with 40 mm (TDL) between the screws yielded the lower stress results. The dynamic locking configuration was simulated in the cracked bone under the larger stress. These were compared to

increases or decreases in stress concentration when the upper distal screw is removed, demonstrating that the stresses would drop considerably. Further analysis of this phenomenon confirmed that the gamma nail slid slightly over the lag screw and cantered over the distal screw causing a reduction the maximum stress concentration in the implant system.

The results were varied in the 125-degree lag screw setup, thereby making the conclusion difficult to verify. Physicians need to establish the types of activities their patient will participate in prior to choosing this lag screw setup. The main disparity in determining screw combination is the critical stress in fractured bone modeled at 400 MPa, limiting the material to approximately 10^7 cycles. There seemed to have no advantage between distal screw combinations and improvements in fatigue failure of this lag screw position. By a purely numerical determination, the two distal screw configuration with 20 mm distance between the screws has the lower stresses in load conditions IV and V. On the other hand, in load condition III and VI, the model with 40 mm separation (TDL) has the lower stress values. The determination breaks down to whether a patient will stand excessive amount or perform actions like walk, climbing stairs or lifting.

In a dynamic locking distal-screw configuration, the two screws separated by 20 mm yielded the lowest stress results. Under load VI, the stress was higher than that of the 40 mm separation configuration. This was not the critical stress in the simulations. Therefore, a reduction of the critical stress was the higher concern. Once the bone has healed, the upper distal screw may be removed. The stress seen in the distal screws are collectively lower than the other two screw combinations. This could be a concern if the patient is very young when the procedure is performed due to numerous other reasons, for example corrosion.

The final lag screw position of 130 degrees produces more concise results than the 125-degree lag screw configuration. These results can provide a guideline for using the distal screw configurations for the 130-degree lag screw position. Determining the distal screw configuration was used in reducing the stress of the gamma nail. Critical stress of the 130-lag screw was modeled with single screw static distal screw. This

model produced a von Mises stress of 300 MPa, which is far below the normal fatigue failure located at approximately 10^8 cycles, producing the lower stress concentrations by an improvement of 20 percent. This enhancement can improve the fatigue failure of the support system. In approximating the improvement, it appears to be an increase of magnitude from 10^8 to 10^9.

In comparing the results from the dynamic locking configuration, it is determined that the screw configuration with 40 mm spacing provides the best results. The static results were slightly elevated but the improvements in the quasi-static loads were beneficial enough to warrant this combination. These results were an improvement of about 20 percent. When returning to a single screw dynamic lock. The stress concentrations increase about 11 percent in load case VI. In load case V, the two-screw configuration is an improvement by about 40 percent over the single screw combination. In this case, it is more advantageous to leave this dynamic locking system in the two-screw configuration. Maintaining this distal screw configuration will ensure that the stresses are at the minimal values for complex loading while also minimizing the number of surgical procedures performed on a patient.

In looking at the von Mises stresses and determining the critical stress, the shear stress is indirectly evaluated. The models and results both demonstrate that the maximum shear stress is concurrent with the von Mises stress proving that minimizing one minimizes the other. Evaluating the results of the model clarifies that the areas of stress are in the distal screws and the holes for the distal screws. The screw combinations improved the shear stress but it is important to address the distal holes themselves. One recommendation not addressed in this study is to fabricate a plug for the hole not in use. This will minimize or eliminate the stresses imparted on these areas.

Overall, this study established that the Gamma III Implant system™ could be improved. To produce an optimized implant system, further studies should be conducted. Future studies should focus on improving the radius of curvature of the gamma nail. Future studies should use calculus-based optimization techniques to vary multiple design parameters simultaneously. Also, future studies should investigate using radiographic inputs to optimize a device optimally configured for a specific fracture pattern. By

evaluating all the configurations of lag screw and distal screws, an informed direction can be imparted to the surgeons, providing the patient with confidence about the procedure and product.

THIS PAGE INTENTIONALLY LEFT BLANK

LIST OF REFERENCES

[1] R.W. Buchoz, J.D. Heckman, C.M. Cort-Brown, K.J. Koval, P. Tornetta III, and M.A. Wirth, "ROCKWOOD AND GREEN'S FRACTURES IN ADULTS VOLUME 2," 6th ed., Lippincott Williams & Wilkins, 2001.

[2] U. Rethnam, J. Cordell-Smith, T. M. Kumar and A. Sing, " Comples Proximal Femoral Fractures in the Elderly Managed Reconstruction Nailing- Complications & Outcomes; a Retros Analysis," journal of Trauma Management and Outcomes, pp. 1-7, Jan 2007.

[3] C. T. Born, J. Maxy, R. Probe, and G Taglang, "Gamma 3TM the compact version of the Gamma Nail System Operative Techniques," Stryker Trauma, USA, LG3-0T, Rev 1, 2004

[4] J. Jolly and Y.W. Kwon, "Impact Analysis of a Biomechanical model," Naval Postgraduate School, Monterey, California, Tech Rep. NPS-ME-00-002, 2000.

[5] R.D. Cook, Malkus, D. S., & Plesha, M. E., *Concepts and Applications of Finite Element Analysis*, 3rd ed., John Wiley & Sons, 1989.

[6] Acoustics, Audio, Video, University of Salford, "Finite Element Method," [online] HTTP;//www.acousticssalford.ac.uk/student_area/bscs/computer-simulation/fem.pdf.

[7] Y. Kwon and H. Bang, "The Finite Element Method Using Matlab," Boca Raton: CRC Press, 2000.

[8] S. Moaveni, "Finite Element Analysis Theory and Application with ANSYS," 3rd ed., New Jersey: Pearson-Prentice Hall, 2008.

[9] H. Gray, "Anatomy of the Human Body," Philadelphia, Len & Febiger, 1918; Bartleby.com, 2000, www.bartleby.com/107 (accessed August 2008).

[10] S. Hoppenfeld and M. Zeide, "Orthopeadic Dictionary," 1st ed. New York: Lippincott-Raven, 1994.

[11] W.D. Callister Jr, "Materials Science and Engineering an Introduction," 7th ed., New York: John Wiley & Sons, Inc., 2007.

[12] All Metals and Forge, LLC, "Titanium"; 1996-2007, [online] Available: http://www.steelforge.com/nonferrous/titanium.htm (accessed August 2008).

[13] The Electolizing Corporation of Ohio, “Titanium Anodizing Provides the Advantages of Hardening and Coloring”: 2008, [online] Available: http://www.Elecrohio.com/finishing/tianodizing/tianodizing.htm (accessed August 2008).

[14] J.H.Keyak, K.B. Skinner and J.A. Fleming, “Effect of force direction on femoral fracture load for two types of loading conditions,” Journal of Orthopedic Research, Vol 19, pp. 539-544, 2001.

[15] K. Sitthiseripratip, H. Van Oosterwyck, J. Vander Sloten, B. Mahaisavariys, E.L.J Bohez, J. Suwanprateeb, R. Van Audekercke, and P. Oris, “Finite Element study of trochateric gamma nail for trochanteric fracture,” Medical Engineering & Physics, vol 25, pp. 99-106, 2003.

[16] C.J. Wang, A.L. Yettram, M.S. Yao an d P. Procter, “Finite Element Analysis of a Gamma Nail with in a Fractured Femur,” Medical Engineering & Physics, vol 20, pp. 677-683, 1998.

[17] H. Lacroix, H. Arwart, C.J. Snijders, and W.P.J. Fontijne, “Preventionof Fracture at the Distal Locking Site of the Gamma Nail,” The Journal of Bone and Joint Surgery, vol. 77, pp.274-276, 1995.

[18] A.C. Ugural and S.K. Fenster, “Advanced Strength and Applied Elasticity” New Jersey: Prentice Hall, 2003.

[19] P.S. Prevey, N. Jayaraman and R. Ravindranalt, “Incorporation of Residual Stresses in Fatigue Performance Desing of Ti-6Al-4V,” In *Proceedings International Conference of Fatigue Damage of Structural Materials* , 2004 (LT paper 253)

APPENDIX

A.1 Single Distal screw

FEM summary data for 130-degree Lag Nail Single Distal Screw

TABLE 1—FE Model Summary

Description	Quantity
Total Nodes	80518
Total Elements	60861
Total Body Elements	49943
Total Contact Elements	10918
Total Spot Weld Elements	0
Element Types	3
Coordinate Systems	0
Materials	2
Thicknesses	0
Layered Composites	0
Rod Properties	0
Bar Properties	0
Beam Properties	0
Curved Pipe Properties	0
Mass Properties	0
Spring Properties	0
Components	0
Contacts	5
Spot Welds	0
Constraint Equations	0
Constraints	1
Forces	1
Pressures	0

TABLE 2—Bodies Summary

Body Name	Nodes	Elements
Solid	44300	27414
Solid	26986	16911
Solid	4895	3006
Solid	4337	2612
Solid	44300	27414
Solid	26986	16911
Solid	4895	3006
Solid	4337	2612
Solid	44300	27414
Solid	26986	16911
Solid	4895	3006
Solid	4337	2612

TABLE 3—Element Types Summary

Generic Element Type Name	ANSYS Name	Description
10 Node Quadratic Tetrahedron	Solid187	10 Node Tetrahedral Structural Solid
Quadratic Triangular Contact	Conta174	3D 8 Node Surface to Surface Contact
Quadratic Triangular Target	Targe170	3D Target Segment

FEM summary data for 125 -degree Lag Nail Single Distal Screw

TABLE 1—FE Model Summary

Description	**Quantity**
Total Nodes	79656
Total Elements	60438
Total Body Elements	49432
Total Contact Elements	11006
Total Spot Weld Elements	0
Element Types	3
Coordinate Systems	0
Materials	2
Thicknesses	0
Layered Composites	0
Rod Properties	0
Bar Properties	0
Beam Properties	0
Curved Pipe Properties	0
Mass Properties	0
Spring Properties	0
Components	0
Contacts	5
Spot Welds	0
Constraint Equations	0
Constraints	1
Forces	1
Pressures	0

TABLE 2—Bodies Summary

Body Name	Nodes	Elements
Solid	41567	25658
Solid	27289	17104
Solid	6463	4058
Solid	4337	2612
Solid	41567	25658
Solid	27289	17104
Solid	6463	4058
Solid	4337	2612

TABLE 3—Element Types Summary

Generic Element Type Name	ANSYS Name	Description
10 Node Quadratic Tetrahedron	Solid187	10 Node Tetrahedral Structural Solid
Quadratic Triangular Contact	Conta174	3D 8 Node Surface to Surface Contact
Quadratic Triangular Target	Targe170	3D Target Segment

FEM summary data for 120-degree Lag Nail Single Distal Screw

TABLE 1—FE Model Summary

Description	**Quantity**
Total Nodes	95263
Total Elements	71728
Total Body Elements	59544
Total Contact Elements	12184
Total Spot Weld Elements	0
Element Types	3
Coordinate Systems	0
Materials	2
Thicknesses	0
Layered Composites	0
Rod Properties	0
Bar Properties	0
Beam Properties	0
Curved Pipe Properties	0
Mass Properties	0
Spring Properties	0
Components	0
Contacts	5
Spot Welds	0
Constraint Equations	0
Constraints	1
Forces	2
Pressures	0

TABLE 2—Bodies Summary

Body Name	Nodes	Elements
Solid	58881	36897
Solid	28917	18186
Solid	3128	1849
Solid	4337	2612
Solid	58881	36897
Solid	28917	18186
Solid	3128	1849
Solid	4337	2612
Solid	58881	36897
Solid	28917	18186
Solid	3128	1849
Solid	4337	2612

TABLE 3—Element Types Summary

Generic Element Type Name	ANSYS Name	Description
10 Node Quadratic Tetrahedron	Solid187	10 Node Tetrahedral Structural Solid
Quadratic Triangular Contact	Conta174	3D 8 Node Surface to Surface Contact
Quadratic Triangular Target	Targe170	3D Target Segment

A.2 Double Distal screw

FEM summary data for 130-degree Lag Nail Double Distal Screw

TABLE 1—FE Model Summary

Description	**Quantity**
Total Nodes	95583
Total Elements	73257
Total Body Elements	59855
Total Contact Elements	13402
Total Spot Weld Elements	0
Element Types	3
Coordinate Systems	0
Materials	2
Thicknesses	0
Layered Composites	0
Rod Properties	0
Bar Properties	0
Beam Properties	0
Curved Pipe Properties	0
Mass Properties	0
Spring Properties	0
Components	0
Contacts	9
Spot Welds	0
Constraint Equations	0
Constraints	1
Forces	2
Pressures	0

TABLE 2—Bodies Summary

Body Name	**Nodes**	**Elements**
Solid	17499	11151
Solid	24772	15553
Solid	4895	3006
Solid	4073	2450
Solid	4137	2498
Solid	40207	25197
Solid	17499	11151
Solid	24772	15553
Solid	4895	3006
Solid	4073	2450
Solid	4137	2498
Solid	40207	25197
Solid	17499	11151
Solid	24772	15553
Solid	4895	3006
Solid	4073	2450
Solid	4137	2498
Solid	40207	25197
Solid	17499	11151
Solid	24772	15553
Solid	4895	3006
Solid	4073	2450
Solid	4137	2498
Solid	40207	25197

TABLE 3—Element Types Summary

Generic Element Type Name	ANSYS Name	Description
10 Node Quadratic Tetrahedron	Solid187	10 Node Tetrahedral Structural Solid
Quadratic Triangular Contact	Conta174	3D 8 Node Surface to Surface Contact
Quadratic Triangular Target	Targe170	3D Target Segment

FEM summary data for 125-degree Lag Nail Double Distal Screw

TABLE 1—FE Model Summary

Description	**Quantity**
Total Nodes	93865
Total Elements	71975
Total Body Elements	58561
Total Contact Elements	13414
Total Spot Weld Elements	0
Element Types	3
Coordinate Systems	0

Materials	2
Thicknesses	0
Layered Composites	0
Rod Properties	0
Bar Properties	0
Beam Properties	0
Curved Pipe Properties	0
Mass Properties	0
Spring Properties	0
Components	0
Contacts	9
Spot Welds	0
Constraint Equations	0
Constraints	1
Forces	2
Pressures	0

TABLE 2—Bodies Summary

Body Name	Nodes	Elements
Solid	15417	9789
Solid	23403	14484
Solid	6463	4058
Solid	4073	2450
Solid	4137	2498
Solid	40372	25282
Solid	15417	9789
Solid	23403	14484
Solid	6463	4058
Solid	4073	2450
Solid	4137	2498
Solid	40372	25282
Solid	15417	9789
Solid	23403	14484
Solid	6463	4058
Solid	4073	2450
Solid	4137	2498
Solid	40372	25282

TABLE 3—Element Types Summary

Generic Element Type Name	ANSYS Name	Description
10 Node Quadratic Tetrahedron	Solid187	10 Node Tetrahedral Structural Solid
Quadratic Triangular Contact	Conta174	3D 8 Node Surface to Surface Contact
Quadratic Triangular Target	Targe170	3D Target Segment

FEM summary data for 120-degree Lag Nail Double Distal Screw

TABLE 1—FE Model Summary

Description	**Quantity**
Total Nodes	93527
Total Elements	70380
Total Body Elements	58458
Total Contact Elements	11922
Total Spot Weld Elements	0
Element Types	3
Coordinate Systems	0
Materials	2
Thicknesses	0
Layered Composites	0
Rod Properties	0
Bar Properties	0
Beam Properties	0
Curved Pipe Properties	0
Mass Properties	0
Spring Properties	0
Components	0
Contacts	5
Spot Welds	0
Constraint Equations	0
Constraints	1
Forces	2
Pressures	0

TABLE 2—Bodies Summary

Body Name	Nodes	Elements
Solid	57409	35973
Solid	28917	18186
Solid	3128	1849
Solid	4073	2450
Solid	57409	35973
Solid	28917	18186
Solid	3128	1849
Solid	4073	2450
Solid	57409	35973
Solid	28917	18186
Solid	3128	1849
Solid	4073	2450

TABLE 3—Element Types Summary

Generic Element Type Name	ANSYS Name	Description
10 Node Quadratic Tetrahedron	Solid187	10 Node Tetrahedral Structural Solid
Quadratic Triangular Contact	Conta174	3D 8 Node Surface to Surface Contact
Quadratic Triangular Target	Targe170	3D Target Segment

INITIAL DISTRIBUTION LIST

1. Defense Technical Information Center
   Ft. Belvoir, Virginia

2. Dudley Knox Library
   Naval Postgraduate School
   Monterey, California

3. Young W. Kwon
   NPS ME Department
   Monterey, California

4. LCDR Stephen Brawley
   Virginia Beach, Virginia

5. Richard Smith
   Spotsylvania, Virginia